FOI
SWEDISH DEFENCE
RESEARCH AGENCY

FOI-R--0410--SE
February 2002
ISSN 1650-1942
Scientific report

M.Sc. Thesis

Jonas Iwarsson

Measurements of strains and strength of laminates with artificial damage

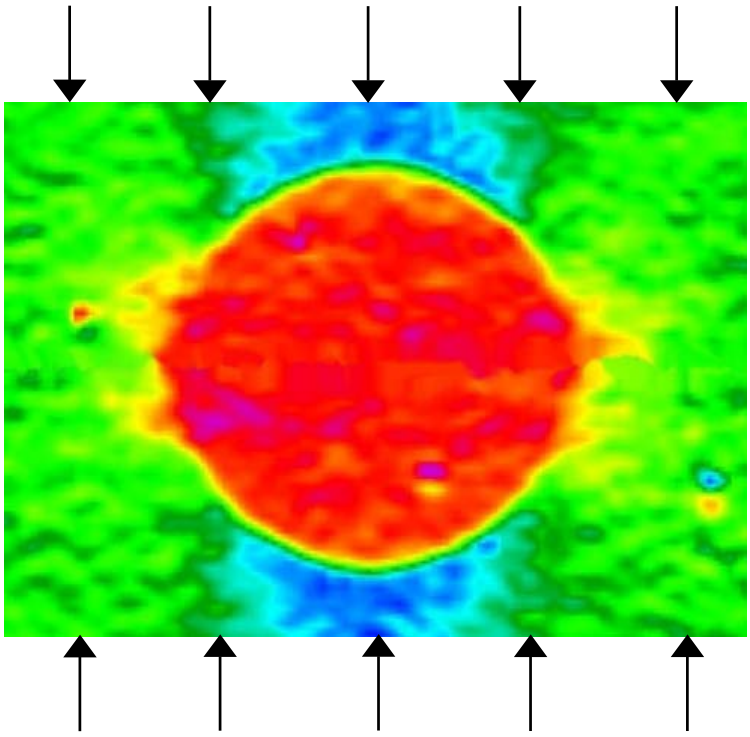

Thesis advisor:

Robin Olsson

Aeronautics Division, FFA
SE-172 90 Stockholm
Sweden

SWEDISH DEFENCE RESEARCH AGENCY

Aeronautics Division, FFA
SE-172 90 Stockholm
Sweden

FOI-R--0410--SE

February 2002

ISSN 1650-1942

Scientific report

Jonas Iwarsson

Measurements of strains and strength of laminates with artificial damage

Issuing organization	**Report number, ISRN**	**Report type**
FOI – Swedish Defence Research Agency Aeronautics Division, FFA SE-172 90 Stockholm Sweden	FOI-R--0410--SE	Scientific report
	Research area code 7. Vehicles	
	Month year February 2002	**Project no.** E824567
	Customers code 5. Contracted Research	
	Sub area code 72. Aeronautical Systems	

Author/s (editor/s)	**Project manager**
Jonas Iwarsson	Robin Olsson
	Approved by Peter Göransson, Head of Aeronautics Division
	Scientifically and technically responsible Robin Olsson

Report title

Measurements of strains and strength of laminates with artificial damage

Abstract (not more than 200 words)

Impact damage may reduce the strength and stiffness of laminated composite structures due to matrix cracking, delaminations and fiber failure. This study is focused on the effect of a local softer region caused by fiber fracture. This region is modeled as a notch – a hole, a soft inclusion or cut fibers.

Several tests were performed in tension and compression with different notch sizes and the strain distributions on the surface were measured optically. The predicted strain and stress distributions for an inclusion in an infinite anisotropic plate were compared with the strain distribution. The point stress and the average stress criteria were used as failure criteria and compensated for finite width. This study showed that the average stress criterion gave a slightly better fit than the point stress criterion.

Two methods for evaluating failure criteria were used – by the failure stress and by the optically measured strain distribution. The conclusion that can be drawn from this study is that the characteristic lengths for these criteria not are material constants; they depend on the load case and on the notch type. One indication of different fracture mechanisms is the difference in the characteristic lengths.

Keywords

Carbon fiber reinforced plastics, composite materials, graphite-epoxy composites, laminates, notch strength, soft inclusions, strain distribution, stress concentration

Further bibliographic information	**Language** English
ISSN 1650-1942	**Pages** 69 p.
	Price acc. to pricelist **Security classification: Open**

Utgivare	Rapportnummer, ISRN	Klassificering
Totalförsvarets Forskningsinstitut - FOI Avdelningen för flygteknik, FFA 172 90 Stockholm	FOI-R--0410--SE	Vetenskaplig rapport
	Forskningsområde 7. Bemannade och obemannade farkoster	
	Månad, år Februari 2002	**Projektnummer** E824567
	Verksamhetsgren 5. Uppdragsfinansierad verksamhet	
	Delområde 72. Flygsystem	
Författare/redaktör Jonas Iwarsson	**Projektledare** Robin Olsson	
	Godkänd av Peter Göransson, Avdelningschef, Flygteknik	
	Tekniskt och/eller vetenskapligt ansvarig Robin Olsson	

Rapportens titel (i översättning)

Töjnings- och hållfasthetsmätningar av laminat med artificiella skador

Sammanfattning (högst 200 ord)

Slagskaror kan minska hållfastheten och styvheten för strukturer av laminerade kompositer på grund av matrissprickor, delamineringar och fiberbrott. Denna studie är fokuserad på ett lokalt vekare område orsakat av fiberbrott. Detta område modelleras som en anvisning – ett hål, en mjuk inneslutning eller med avskurna fibrer.

Ett antal prov utfördes både i drag och i tryck med olika anvisningsstorlekar och töjningsfältet på ytan mättes optiskt. Töjnings- och spänningsfördelningen för en inneslutning i en oändlig anisotrop platta jämfördes med den optiskt uppmätta töjningsfördelningen. Punkt- och medelspänningskriteriet användes som brottkriterier och var kompenserade för finit bredd. Denna studie visade att medelspänningskriteriet gav något bättre överensstämmelse än punktspänningskriteriet.

Två metoder för att utvärdera brottkriterierna användes – genom brottspänningen eller med den optiskt uppmätta töjningsfördelningen. Slutsatsen som kan dras är att de karakteristiska längderna för de nämnda kriterierna inte är materialkonstanter utan att de beror på lastsituation och typ av anvisning. En indikation på olika brottmekanismer är skillnaden i karakteristisk längd.

Nyckelord

Kolfiberarmerade plaster, kompositmaterial, kolfiber/epoxikompositer, laminat, anvisningshållfasthet, mjuka inneslutningar, töjningsfördelning, spänningskoncentration

Övriga bibliografiska uppgifter	**Språk** Engelska
ISSN 1650-1942	**Antal sidor:** 69 s.
Distribution enligt missiv	**Pris: Enligt prislista** **Sekretess: Öppen**

Contents

Nomenclature

List of the most important parameters in this report:

a_0	Characteristic length, average stress criterion
a_{ij}	Compliance matrix components
A_{ij}	Stiffness matrix components
b_i, c_i	Constants for strain or stress field approximations
d_0	Characteristic length, point stress criterion
D	Notch diameter
E	Young's modulus
G	Shear modulus
K_T	Stress concentration factor, finite plate
K_T^∞	Stress concentration factor, infinite plate
$K_{\varepsilon,T}$	Strain concentration factor, finite plate
$K_{\varepsilon,T}^\infty$	Strain concentration factor, infinite plate
R	Inclusion or hole radius
W	Specimen width
Y	Finite width correction factor
ε_x	Strain in the *x*-direction, finite plate
ε_{ff}	Far field strain, finite plate
ε_{local}	Strain at the notch edge
μ_1, μ_2	Complex roots
ν	Poisson's ratio
σ_0	Unnotched failure stress
σ_N	Notched failure stress
σ^∞	Applied stress
σ_x	Stress in the *x*-direction, finite plate
σ_x^∞	Stress in the *x*-direction, infinite plate
σ_{low}	Low load level, used for comparisons

Definition of the specimen numbering:

$\underbrace{\text{T}}_{i}\underbrace{020}_{ii}/\underbrace{10}_{iii}-\underbrace{2}_{iv}$ (Specimen 2 tested in tension with a 10 mm inclusion)

i Loading
- T: Tension
- C: Compression

ii Stiffness ratio in % of the notch over the laminate
- 000: Hole (0 %)
- 020: Inclusion (20 %)
- 100: Unnotched (100 %)
- CUT: Laminate with cut fibers

iii Notch diameter: 0, 5, 10 or 20 mm

iv Specimen number: 1, 2 or 3

1. Introduction

Impact damage may reduce the strength and stiffness of laminated composite structures. Extensive experimental studies on impacted laminates have been performed, as described for example by Abrate (1991), Olsson (1999) and Sjögren (1999). The impact commonly results in matrix cracking, delaminations and fiber failure. This study is focused on the effect of local softer regions caused for example by fiber fracture.

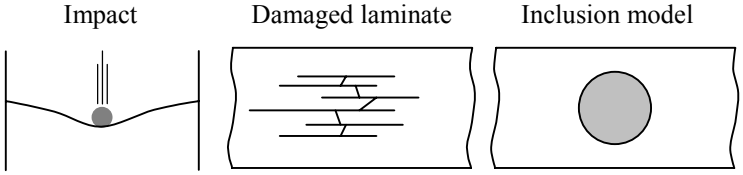

Figure 1.1 Simulation of impacted laminate.

The most common method to simulate an impacted laminate is to treat the damaged region as a soft inclusion (Figure 1.1), but most previous studies have been on hard inclusions in laminates, Tan (1994).

Sjögren (1999) impacted several laminates and studied them through fractography, but in Sjögren et al. (2001) pieces from the damaged region of an impacted laminate were cut out and tested it in tension and compression to determine the stiffness degradation of the impacted region. In the most damaged region with fiber breakage, delaminations and matrix cracks the tensile modulus decreased by about 80 % and the compressive modulus decreased by about 50 % for a 16-ply laminate. For this case the radius of the most damaged region was determined by fractography to be about 5 mm. The broken fibers may take load in compression, which gives higher stiffness in compression than in tension.

The theoretical solutions for an inclusion in a laminate were derived in Lekhnitskii (1968) and Tan (1994). When dealing with a hole in an infinitely brittle material the failure stress is one third of the unnotched failure stress, while an infinitely tough material will not be affected at all (Figure 1.2). The use of an inclusion is common in repair methods thanks to the reduction in stress concentration factor, Tan (1994).

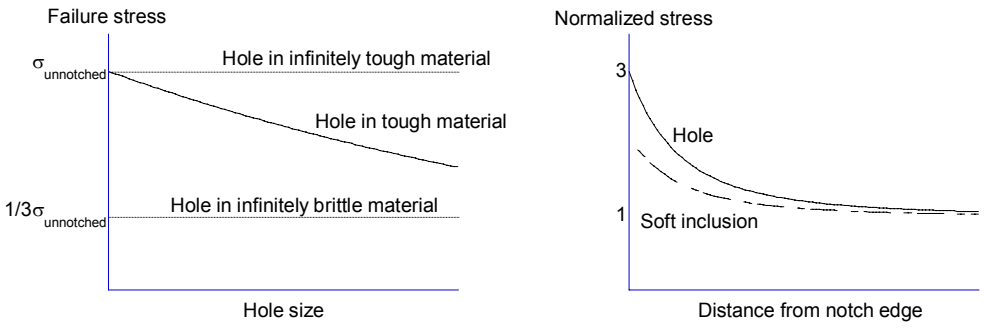

Figure 1.2 Toughness sensitivity and stress reduction.

Prior to this study several finite element (FE) calculations of laminates with inclusions have been performed, both here at FOI/FFA and in the references, for example by Dost et al. (1988), Gillespie and Carlsson (1988) and Xiong (1994). To verify the FE-calculations through experiments, an inverse finite element (IFE) method is available. The IFE method calculates the elastic properties of the specimen and the inclusion from a given whole field strain distribution.

To deal with the toughness in the material, the point stress and the average stress criterion assumes that failure of the notched specimen will occur when the stress at some point, or when the average stress over some region exceeds the failure stress, respectively. It is assumed that the characteristic lengths given by the point stress and the average stress criterion may be used as material constants, not depending on the load and notch type, Tan (1994). However, due to different failure mechanisms for laminated composites – matrix cracking and fiber fracture in tension and fiber kinking in compression – the characteristic lengths in tension and compression are expected to be different. For an inclusion in a laminate, the fibers close to the inclusion are supported by the inclusion, but for a hole in a laminate, the fibers may kink into the open hole. Hence, a notch dependency of the characteristic lengths is possible.

The purpose of this report is to collect an experimental foundation for:
- Validation of an inverse FE-method through optical measurements.
- Comparison of failure mechanisms.
- Validation of failure criteria or guidelines for their development.

2. Theory

2.1 Stress distribution

2.1.1 Hole

An infinite orthotropic plate with a circular hole of radius R is subjected to uniform uniaxial stress, σ^{∞}, see Figure 2.1.

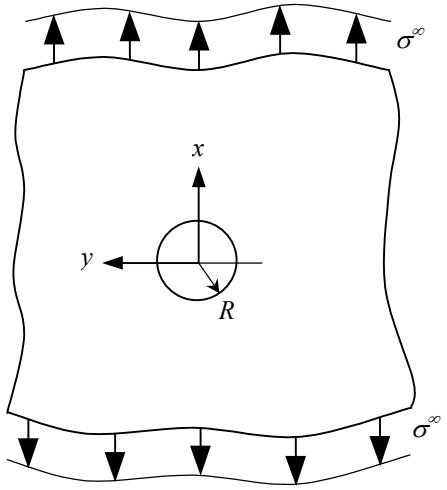

Figure 2.1 Infinite orthotropic plate with circular hole.

Along the y-axis the normal stress, $\sigma_x^{\infty}(x,y)$, in the loading direction can be approximately expressed as given by Konish and Whitney (1975):

$$\sigma_x^{\infty}(0,y)=\frac{\sigma^{\infty}}{2}\left(2+\left(\frac{R}{y}\right)^2+3\left(\frac{R}{y}\right)^4-\left(K_{T,H}^{\infty}-3\right)\left[5\left(\frac{R}{y}\right)^6-7\left(\frac{R}{y}\right)^8\right]\right) \quad (2.1)$$

for $|y|\geq R$, where $K_{T,H}^{\infty}$ is the stress concentration factor for a hole in an orthotropic plate, expressed as in Awerbuch and Madhukar (1985):

$$K_{T,H}^{\infty}=1+\sqrt{\left(\frac{2}{A_{22}}\left(\sqrt{A_{11}A_{22}}-A_{12}+\frac{A_{11}A_{22}-A_{12}^2}{2A_{66}}\right)\right)} \quad (2.2)$$

where A_{ij} are the in-plane stiffness matrix components of the orthotropic laminate where the 1-direction coincides with the load direction. Note the incorrect definition of the 1-direction in Awerbuch and Madhukar (1985)

and several other references. In terms of engineering constants Equation (2.2) may be written as:

$$K_{T,H}^{\infty} = 1 + \sqrt{2\left(\sqrt{\frac{E_x}{E_y}} - \nu_{xy}\right) + \frac{E_x}{G_{xy}}} \tag{2.3}$$

For a quasi-isotropic laminate $K_{T,H}^{\infty} = 3$, as in the isotropic case and Equation (2.1) reduces to:

$$\sigma_x^{\infty}(0,y) = \sigma^{\infty}\frac{1}{2}\left(2 + \left(\frac{R}{y}\right)^2 + 3\left(\frac{R}{y}\right)^4\right) \tag{2.4}$$

2.1.2 Inclusion

The stress distribution in an anisotropic plate subjected to uniform uniaxial stress and containing an elliptical inclusion, see Figure 2.2, can be analyzed using the complex variable approach proposed by Lekhnitskii (1968).

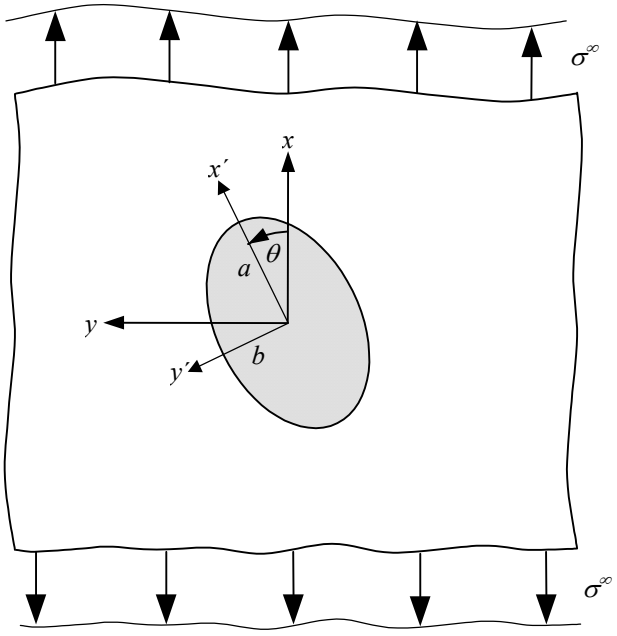

Figure 2.2 Infinite anisotropic plate with elliptical inclusion.

The major and minor axes of the ellipse are denoted as a and b, respectively. θ denotes the angle between the x-axis and the major axis of

the ellipse, where the loading direction is parallel to the *x*-axis. The evenly distributed far-field stress in the infinite plate is denoted by σ^{∞}.

The stress in the *x*-direction was expressed by Xiong (1994), note the sign error in Equation (2) in Xiong (1994). The stress should be expressed as follows:

$$\sigma_x^{\infty} = \sigma^{\infty} - 2\sum_{k=1}^{2} \mathrm{Re}\left[\frac{\overline{\varphi}_k \left(\mu_k \cos\theta + \sin\theta\right)^2}{a + i\mu_k b} \left(\frac{z_k}{\sqrt{z_k^2 - a^2 - \mu_k^2 b^2}} - 1 \right) \right] \tag{2.5}$$

where

$$\left.\begin{aligned} \overline{\varphi}_1 &= \frac{1}{2(\mu_1 - \mu_2)} \left[\left(A' - \sigma^{\infty} \cos^2\theta\right) bi - \left(B' - \sigma^{\infty} \sin^2\theta\right) \mu_2 a \right. \\ &\quad \left. - \left(C' + \sigma^{\infty} \sin\theta\cos\theta\right)\left(a - i\mu_2 b\right) \right] \\ \overline{\varphi}_2 &= \frac{-1}{2(\mu_1 - \mu_2)} \left[\left(A' - \sigma^{\infty} \cos^2\theta\right) bi - \left(B' - \sigma^{\infty} \sin^2\theta\right) \mu_1 a \right. \\ &\quad \left. - \left(C' + \sigma^{\infty} \sin\theta\cos\theta\right)\left(a - i\mu_1 b\right) \right] \\ z_k &= \left(x\cos\theta + y\sin\theta\right) + \mu_k \left(-x\sin\theta + y\cos\theta\right) \end{aligned}\right\} \tag{2.6}$$

and A', B' and C' are the two normal and one shear stress components in the inclusion in the x'-y' system and i is the imaginary unity. μ_1 and μ_2 are the two different complex roots, with positive imaginary part, of the characteristic equation:

$$a_{11}\mu^4 - 2a_{16}\mu^3 + \left(2a_{12} + a_{66}\right)\mu^2 - 2a_{26}\mu + a_{22} = 0 \tag{2.7}$$

where a_{ij}, i,j = 1,2,6 denotes the compliances of the laminate where the 1-direction coincides with the load direction. Note that $\mu_1 = \mu_2 = i$ for quasi-isotropic laminates.

For an orthotropic laminate with a non-inclined inclusion ($\theta = 0$) A', B' and C' can be expressed as given by Tan (1994):

$$\left.\begin{aligned} A = A' &= \frac{\sigma^{\infty}}{H} \left[a_{11}a_{22}\left(k + n\right) + a_{11}a'_{22}k\left(1 + n\right) + a_{22}\left(a_{12} + a_{66} + a'_{12}\right) \right] \\ B = B' &= \frac{\sigma^{\infty}}{H} \left[a_{22}\left(a_{11} - a'_{11}\right) + a_{11}k\left(a_{12} - a'_{12}\right)\left(1 + n\right) \right] \\ C = C' &= 0 \end{aligned}\right\} \tag{2.8}$$

where a'_{ij}, i,j = 1,2,6 denotes the compliances of the inclusion and

$$\left.\begin{aligned} H &= (a_{11}a_{22} + a'_{11}a'_{22})k + a_{22}(a_{66} + 2a'_{12}) \\ &\quad + (a_{11}a'_{22}k + a_{22}a'_{11})n - (a_{12} - a'_{12})^2 k \\ k &= -\mu_1\mu_2 = \sqrt{\frac{a_{22}}{a_{11}}} \\ n &= -i(\mu_1 + \mu_2) = \sqrt{\frac{2a_{12} + a_{66}}{a_{11}} + 2\sqrt{\frac{a_{22}}{a_{11}}}} \end{aligned}\right\} \tag{2.9}$$

Equation (2.5) can be used for all types of laminates, both anisotropic and quasi-isotropic, but for the isotropic case the equation includes singularities since $\mu_1 = \mu_2 = i$. These singularities give equations with both denominator and numerator equal to zero, that can be avoided in two ways: either by using L'Hospital's rule or by introducing a small imaginary number, δ, and using limits:

$$\left.\begin{matrix} \mu_1 \\ \mu_2 \end{matrix}\right\} = \lim_{\delta \to 0} \begin{cases} i + \delta \\ i - \delta \end{cases} \tag{2.10}$$

An alternative way to evaluate the quasi-isotropic case is to use the stress field in an isotropic plate containing a cylindrical isotropic inclusion, which is derived for plain strain in Goodier (1933). The stresses in the loading direction and perpendicular to the loading direction, respectively, on the y-axis can then be expressed as:

$$\sigma_x^{\infty}(0,y) = \sigma^{\infty}\frac{1}{2}\left(c_1 + c_2\left(\frac{R}{y}\right)^2 + c_3\left(\frac{R}{y}\right)^4\right) \tag{2.11a}$$

$$\sigma_y^{\infty}(0,y) = \sigma^{\infty}\frac{1}{2}\left(\left(-c_2 + \frac{4}{3}c_3\right)\left(\frac{R}{y}\right)^2 - c_3\left(\frac{R}{y}\right)^4\right) \tag{2.11b}$$

where R is the radius of the inclusion ($a = b = R$ in Figure 2.2) and the constants for plane strain ($\varepsilon_z = 0$) are:

$$\left.\begin{aligned} c_1 &= 2 \\ c_2 &= \frac{(1-2\nu')(1+\nu')E - (1-2\nu)(1+\nu)E'}{(1-2\nu')(1+\nu')E + (1+\nu)E'} \\ c_3 &= 3\frac{(1+\nu')E - (1+\nu)E'}{(1+\nu')E + (3-4\nu)(1+\nu)E'} \end{aligned}\right\} \tag{2.12}$$

E and E' are Young's modulus for the plate and the plate, respectively, ν and ν' are Poisson's ratio for the plate and the inclusion, respectively. Note the notation in Goodier (1933) where σ is Poisson's ratio and μ is the shear modulus.

The relations between plane strain and plane stress may be used to derive the stress distribution in an isotropic plate containing a cylindrical isotropic inclusion under plane stress conditions. The relation was given by Fung (1965) as follows:

$$\left.\frac{1}{1-2\nu}\right|_{\text{Plane strain}} = \left.\frac{1+\nu}{1-\nu}\right|_{\text{Plane stress}} \tag{2.13}$$

Combining Equations (2.11), (2.12) and (2.13) expressions for the stress distributions can be derived where the constants for plane stress ($\sigma_z = 0$) are:

$$\left.\begin{aligned} c_1 &= 2 \\ c_2 &= \frac{(1-\nu')E-(1-\nu)E'}{(1-\nu')E+(1+\nu)E'} \\ c_3 &= 3\frac{(1+\nu')E-(1+\nu)E'}{(1+\nu')E+(3-\nu)E'} \end{aligned}\right\} \tag{2.14}$$

It was verified that Equation (2.5) for quasi-isotropic laminates and Equation (2.11a) for plane stress yield identical results for quasi-isotropic laminates.

For a hole, $E' = 0$, which yields $c_1 = 2$, $c_2 = 1$, $c_3 = 3$ and Equation (2.11a) equals Equation (2.4).

The relationship between strain and stress under plane stress conditions for an infinite and isotropic material is, Sundström (1998):

$$\frac{\varepsilon_x^{\infty}(0,y)}{\varepsilon^{\infty}} = \frac{1}{\sigma^{\infty}}\left(\sigma_x(0,y)-\nu\sigma_y(0,y)\right) \tag{2.15}$$

The normalized strain distribution in the loading direction along the y-axis for plane stress ($\sigma_z = 0$) can then be expressed as:

$$\frac{\varepsilon_x^{\infty}(0,y)}{\varepsilon^{\infty}} = \frac{1}{2}\left(c_1+\left((1+\nu)c_2-\frac{4}{3}\nu c_3\right)\left(\frac{R}{y}\right)^2+(1+\nu)c_3\left(\frac{R}{y}\right)^4\right) \tag{2.16}$$

where ε^{∞} is the applied strain, ν is Poisson's ratio for the laminate and the constants c_i from Equation (2.14) are valid.

2.2 Finite width correction factor

Since most equations are derived for infinite plates it is relevant to introduce a finite width correction factor which corrects the infinite plate solution to apply for a plate specimen of width W, see Figure 2.3.

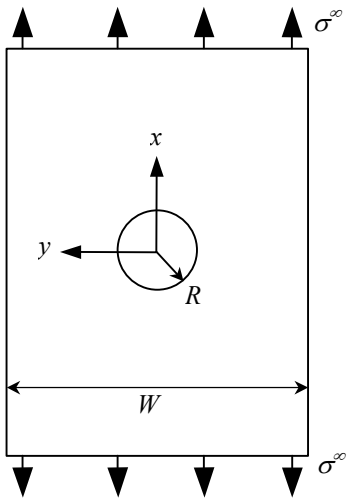

Figure 2.3 Orthotropic plate of finite width with central circular hole.

To derive a finite width correction factor it is assumed that the stress profile in the finite plate is identical to that in an infinite plate, except for a constant correction factor, Y, Tan (1994):

$$\sigma_x(0,y) = Y\sigma_x^{\infty}(0,y) \tag{2.17}$$

A method used in the literature for example by Awerbuch and Madhukar (1985), Tan (1994) and Gillespie and Carlsson (1988), to relate the experimental notched strength, σ_N, for laminates with finite width to the corresponding for infinite laminates, σ_N^{∞}, is to use a correction factor:

$$\frac{\sigma_N^{\infty}}{\sigma_N} = \frac{K_T}{K_T^{\infty}} = Y \tag{2.18}$$

where Y is the finite width correction factor, K_T and K_T^{∞} denote the stress concentration factors for the finite and the infinite plate, respectively.

2.2.1 Hole

The finite width correction factor, Y_H, for an orthotropic plate with a hole, see Figure 2.3, can be expressed as given by Tan (1994):

$$\left.\begin{aligned} \frac{1}{Y_H} &= \frac{K^{\infty}_{T,H}}{K_{T,H}} = \frac{3(1-2R/W)}{2+(1-2R/W)^3} \\ &\quad + \frac{1}{2}\left(\frac{2R}{W}M\right)^6 \left(K^{\infty}_{T,H}-3\right)\left[1-\left(\frac{2R}{W}M\right)^2\right] \\ M^2 &= \frac{\sqrt{1-8\left(\frac{3(1-2R/W)}{2+(1-2R/W)^3}-1\right)}-1}{2(2R/W)^2} \end{aligned}\right\} \qquad (2.19)$$

where $K^{\infty}_{T,H}$ is the stress concentration factor for the orthotropic plate with infinite width, given by Equation (2.2).

For the quasi-isotropic plate $K^{\infty}_{T,H} = 3$ and Equation (2.19) reduces to:

$$Y_H = \frac{K_{T,H}}{K^{\infty}_{T,H}} = \frac{2+(1-2R/W)^3}{3(1-2R/W)} \qquad (2.20)$$

which is plotted in Figure 2.4 where $D = 2R$.

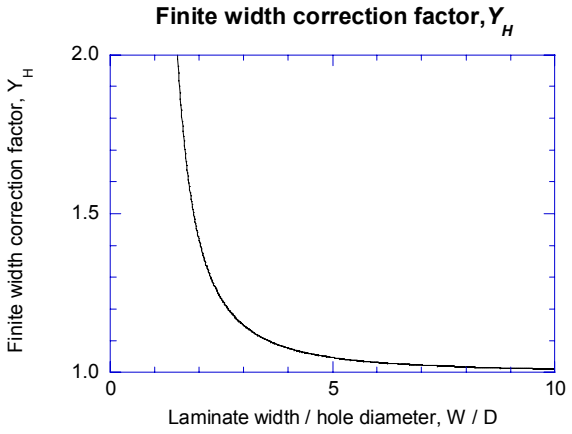

Figure 2.4 Finite width correction factor, Y_H, for hole in a quasi-isotropic laminate.

The assumption made in the previous procedure was that the stress distribution profile for a finite plate is identical to that for an infinite plate

except for the finite width correction factor, Y_H, in a small highly stressed region $R \le x \le d_0 + R$, Gillespie and Carlsson (1988):

$$\frac{\sigma_x(0,y)}{\sigma_x^{\infty}(0,y)} = Y_H \qquad \text{where} \begin{cases} R \le y \le d_0 + R \\ \sigma_x(0, R + d_0) = \sigma_0 \end{cases} \tag{2.21}$$

where σ_0 is the failure stress of the unnotched laminate.

With this method the entire stress field cannot be calculated. To improve Equation (2.21) Gillespie and Carlsson (1988) introduced a function $\delta(x)$ with the properties

$$\delta(y = R) = 0 \quad \text{and} \quad -1 \le \delta(y > R) \le 0 \tag{2.22}$$

so that

$$\frac{\sigma_x(0,y)}{\sigma_x^{\infty}(0,y)} = Y_H(1 + \delta(y)) \tag{2.23}$$

where $\delta(y)$ can be approximately expressed as:

$$\delta(y) = -c(y - R)(Y_H - 1) \tag{2.24}$$

The constant, c, was determined by Gillespie and Carlsson (1988), through curve fitting techniques and finite element analysis of different orthotropic carbon/epoxy laminates to be $c = 0.070\ \text{mm}^{-1}$, for $2 \le W / D \le 4$.

By using Equations (2.23) and (2.24) the stress field for an infinite plate can be expressed as a function of the coordinate y and actual stress of the finite plate:

$$\sigma_x^{\infty}(0,y) = \frac{\sigma_x(0,y)}{Y_H(1 - c(y - R)(Y_H - 1))} \tag{2.25}$$

2.2.2 Inclusion

The finite width correction factor, Y_I, for an anisotropic plate of width W containing an elliptical inclusion (see Figure 2.5) was derived in Xiong (1994).

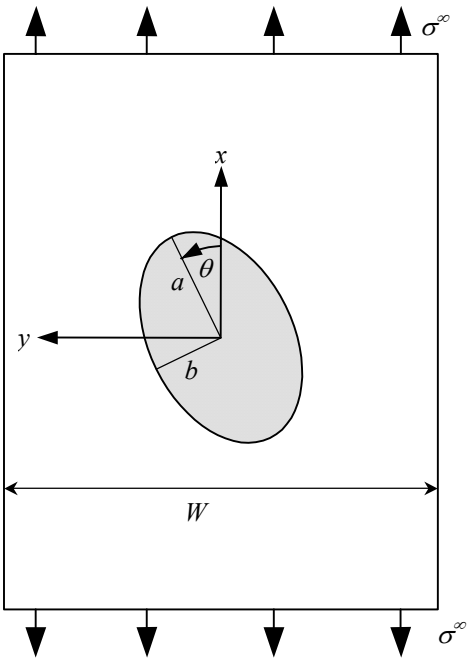

Figure 2.5 Finite anisotropic plate with elliptical inclusion.

To simplify the equations the finite width correction factor, Y_I, is presented for a non-inclined ellipse, $\theta = 0$. Note the misprints in Equation (6) in Xiong (1994) and in Equation (10) in Xiong et al. (1995), the inverse finite width correction factor should instead be expressed:

$$\left.\begin{aligned}\frac{1}{Y_I} = M\left(1-\frac{2b}{W}+\frac{2}{\sigma^{\infty}W}Ab\right) \\ -\frac{4M}{\sigma^{\infty}W}\sum_{k=1}^{2}\mathrm{Re}\left[\frac{\overline{\varphi}_k\mu_k}{a+i\mu_k b}\left(\sqrt{\left(\mu_k\frac{W}{2}\right)^2-a^2-\mu_k^2b^2}\right.\right. \\ \left.\left.-ia-\mu_k\left(\frac{W}{2}-b\right)\right)\right]\end{aligned}\right\} \quad (2.26)$$

where $\overline{\varphi}_k$, μ_k and A are expressed in Equations (2.6), (2.7), and (2.8), respectively, and M is:

$$M = \left[\left(\frac{3(1-2b/W)}{2+(1-2b/W)^3}\right)\Big/\left(1-\frac{1}{2}\left(\frac{2b}{W}\right)^2-\frac{1}{2}\left(\frac{2b}{W}\right)^4\right)\right]^{(1-M_r)^3} \quad (2.27)$$

where M_r is the stiffness ratio of the inclusion over the laminate.

Equation (2.26) contains singularities of the same kind as Equation (2.5) and they can be overcome in the same way, i.e. by using L'Hospital's rule or by using limits.

An alternative expression, based on finite element experiments of the finite width correction factor for quasi-isotropic carbon/epoxy plates containing a circular inclusion of radius R was presented by Dost et al. (1988):

$$Y_I = \left[\frac{2 + \left(1 - \frac{2R}{W}\right)^3}{3\left(1 - \frac{2R}{W}\right)} \right]^{\left(1 - M_r^{0.722}\right)^{2.56}} \tag{2.28}$$

where M_r is the stiffness ratio of the inclusion over the laminate.

2.3 Failure criteria

Two criteria for predicting the notched strength have been proposed by Nuismer and Whitney: the point stress criterion (PSC) and the average stress criterion (ASC).

The point stress criterion states that failure will occur when the stress, $\sigma_x(0,y)$, at some distance, d_0, away from the stress concentration reaches the unnotched strength of the laminate, Nuismer and Whitney (1975):

$$\sigma_x^{\infty}(0,y)\Big|_{y=R+d_0} = \sigma_0 \tag{2.29}$$

where R is the radius of the notch, $R = D / 2$.

The average stress criterion assumes that failure will occur when the average value of the stress, σ_x, over some distance, a_0, reaches the unnotched strength for the laminate, Nuismer and Whitney (1975):

$$\frac{1}{a_0}\int_R^{R+a_0} \sigma_x^{\infty}(0,y)dy = \sigma_0 \tag{2.30}$$

For a quasi-isotropic laminate, where the stress distribution along the y-axis is given by Equation (2.11a), the point stress criterion for a finite plate can be expressed as:

$$\left.\begin{aligned}\frac{\sigma_N}{\sigma_0} &= \frac{1}{Y}\frac{2}{c_1 + c_2\xi_1^2 + c_3\xi_1^4} \\ \xi_1 &= \frac{R}{R + d_0}\end{aligned}\right\} \tag{2.31}$$

and the average stress criterion can be expressed as:

$$\left.\begin{aligned}\frac{\sigma_N}{\sigma_0} &= \frac{1}{Y}\frac{2}{c_1 + c_2\xi_2 + c_3\xi_2^3\left(1 + \frac{a_0}{R} + \frac{1}{3}\left(\frac{a_0}{R}\right)^2\right)} \\ \xi_2 &= \frac{R}{R + a_0}\end{aligned}\right\} \tag{2.32}$$

where c_i, $i = 1,2,3$, are constants depending on the relative inclusion stiffness. Expressions for c_i can be found in Equation (2.12) for plane strain and in Equation (2.14) for plane stress. For a hole these constants are $c_1 = 2$, $c_2 = 1$ and $c_3 = 3$, according to Equation (2.4), and Equations (2.31) and (2.32) reduce to, respectively:

$$\begin{aligned}\text{PSC}: \quad & \frac{\sigma_{N,H}}{\sigma_0} = \frac{1}{Y_H}\frac{2}{2 + \xi_1^2 + 3\xi_1^4} \\ \text{ASC}: \quad & \frac{\sigma_{N,H}}{\sigma_0} = \frac{1}{Y_H}\frac{2(1 - \xi_2)}{2 - \xi_2^2 - \xi_2^4}\end{aligned} \tag{2.33}$$

3. Specimens

3.1 Laminate

The laminate consisted of 24 layers carbon fiber/epoxy prepreg, Hexcel HTA/6376C, with quasi-isotropic lay-up sequence $[0/\pm45/90]_{3S}$. Each ply had the nominal properties according to Olsson (2000) listed in Table 3.1.

Table 3.1 Nominal ply properties.

Thickness [mm]	Elastic moduli [GPa]			Poisson's ratio
t_{ply}	E_{11}	E_{22}	G_{12}	ν_{12}
0.13	140	10	5.2	0.3

Previous experiments have shown that $E_{11} = 131$ GPa for compression and $E_{11} = 143$ GPa for tension. It will further be discussed which of these three moduli that suits this laminate. By using the laminate theory in Zenkert and Battely (1996) Table 3.1 gives the laminate the theoretical quasi-isotropic properties listed in Table 3.2.

Table 3.2 Nominal properties of the laminates.

Thickness [mm]	Elastic moduli [GPa]		Poisson's ratio
t_{theory}	E_{theory}	G_{theory}	ν_{theory}
3.12	54.2	20.7	0.31

(If $E_{11} = 131$ GPa is used then $E_{theory} = 51.3$ GPa and if $E_{11} = 143$ GPa then $E_{theory} = 55.2$ GPa.)

Sicomp AB and Mekpart AB had manufactured three different sizes of the laminates – small, medium and large. The geometry, see Figure 3.1, and exact sizes of the specimens were measured and the average values are listed in Table 3.3, where L_{eff} is the approximate distance between the clamps in the loading machine and t is the effective load bearing thickness.

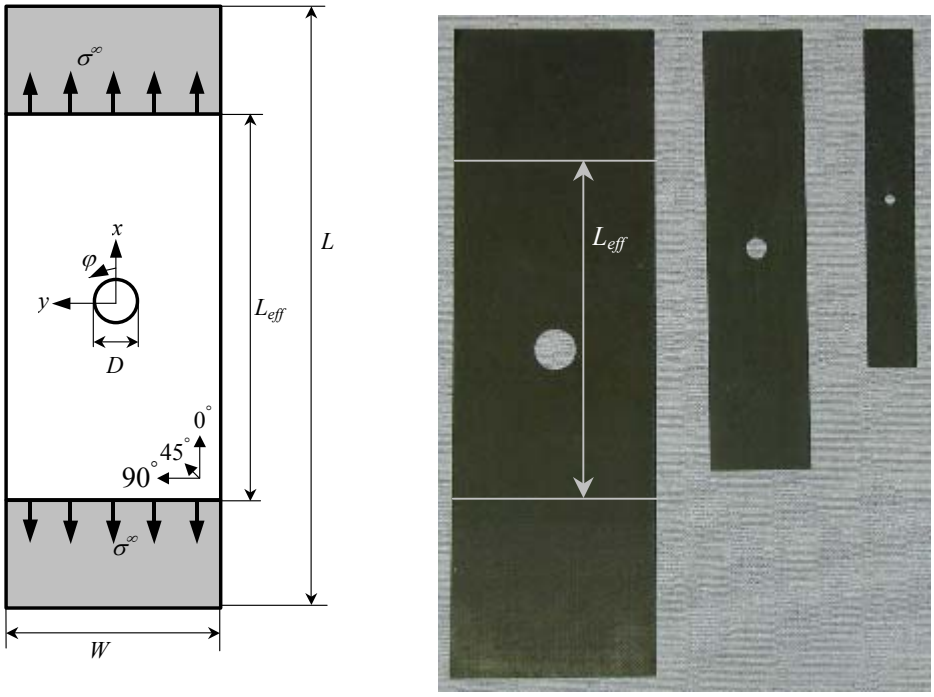

Figure 3.1 Specimen geometry and relative sizes.

Measurements done by scraping off the surplus matrix material knobbles on the surface showed that the effective thickness could be obtained by subtracting 0.09 mm from the measured thickness, $t_{measured}$, i.e.:

$$t = t_{measured} - 0.09\,[\text{mm}]$$

Table 3.3 Specimen dimensions [mm].

Size	Notch size $D = 2R$	Thickness t	Width W	Effective length L_{eff}
Small	5	3.05	25.1	50
Medium	10	3.06	50.1	100
Large	20	3.05	99.4	200

3.2 Notches

The laminates had been manufactured in four types, Table 3.4, – three notched types and one unnotched.

Table 3.4 Notch types.

Notch type	Description
Hole	A hole drilled, or cut out with water-jet. Diameters 5, 10 and 20 mm.
Inclusion	An inclusion with approximately 20 % of the laminate stiffness filled in the hole. Diameters 5, 10 and 20 mm.
Cut fibers	The fibers in each ply were cut perpendicular to the fiber direction. Cut lengths 5, 10 and 20 mm.
Unnotched	Reference for measuring failure stress, strain and the elastic modulus *E*.

The soft inclusion consisted of epoxy with 50 % glass beads, Sjögren (2001). The nominal properties obtained in tests on larger panels of the material are given in Table 3.5.

Table 3.5 Nominal properties of the inclusion material.

Load case	Tension	Compression
Young's modulus [GPa]	11.7	12.6
Poisson's ratio	0.3	
Max stress [MPa]	54.5	144.8
Strain at max stress [%]	0.54	2.5

The behavior of the inclusion material in compression tends to be plastic for strain levels over 0.5 %.

4. Mechanical testing

4.1 Test program

The tests were performed according to Table 4.1.

Table 4.1 Test program.

Load case	Tension				Compression			
Notch size [mm]	0	5	10	20	0	5	10	20
Specimen width [mm]	25	25	50	100	25	25	50	100
Hole		3	3	3		3	2	2
Inclusion				3		3	2	2
Cut fibers			3	3			2	2
Unnotched	3				3			

The numerals inside the table indicate the number of performed test of each specimen configuration, i.e. two tests were performed in compression with 10 mm inclusion.

To reduce evaluation time, considering the relatively small scatter in results, the number of compression tests on medium and large size specimens was reduced from 3 to 2 per case.

The specimens are denoted by a letter which describes the load case, a number or letters to describe the notch type, a number which describes the notch size and a specimen number:

$\underbrace{C}_{i}\underbrace{100}_{ii}/\underbrace{0}_{iii}-\underbrace{3}_{iv}$ (*)

i Loading
T: Tension
C: Compression

ii Stiffness ratio in % of the notch over the laminate
000: Hole (0 %)
020: Inclusion (20 %)
100: Unnotched (100 %)
CUT: Laminate with cut fibers

iii Notch diameter: 0, 5, 10 or 20 mm

iv Specimen number: 1, 2 or 3

The example (*) is unnotched specimen 3 tested in compression, width 25 mm.

4.2 Equipment

The specimens were equipped with both strain gages and white spray paint. The spray paint was used for the optical measurements (DSP), which will be described in Chapter 5.

For each specimen of width 50 mm or 100 mm five or six 5 mm strain gages were used. The strain gage type was KFG-5-120-C1-11L3M3R, manufactured by Kyowa Electronic Instruments. The locations of the gages on the laminate are shown in Figure 4.1. Gages 1, 2, 3 and 4 were placed on the edge of the specimen and gages 5 and 6 on the surface. Gage 6 is placed on the opposite side of gage 5. Before testing of the laminates some other tests had been done to verify that the gages on the edge of the laminate gave the same results as gages close to the edge, but on the back and front surface.

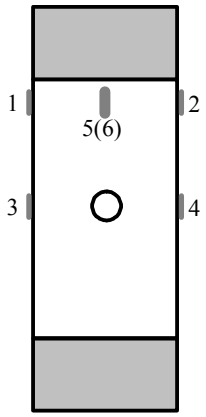

Figure 4.1 Placement of the strain gages.

The gages 1, 2, 5 and 6 were used to determine if the strain was evenly distributed over the width, gages 3 and 4 were used to determine the edge strain in the notched section. Gages 3 and 4 were also used to verify that the specimen was symmetrically mounted in the test machine.

For the small specimens, 25 mm width, only two strain gages in the notched section (3 and 4 in Figure 4.1) were applied. The same type of gages as for the larger specimens were used, except for C020/5-1,2,3 where 2 mm gages of type KFG-2-120-C1-11L3M3R were used.

Ordinary matt white spray paint was applied to the specimens. The paint was gently sprayed to create a random pattern of white dots on the surface of the black laminate. During testing of the specimen this pattern was photographed using DSP (Digital Speckle Photography). DSP is based on the observation of the displacements of a random pattern on the

surface of the specimen. From the displacements the strains on the surface are calculated. See Chapter 5 for further details.

Since the cameras needed extra light for the exposition ordinary desk lamps with 60 W light bulbs were used. Specimens with dotted pattern and the experimental setup are shown in Figure 4.2 and 4.3.

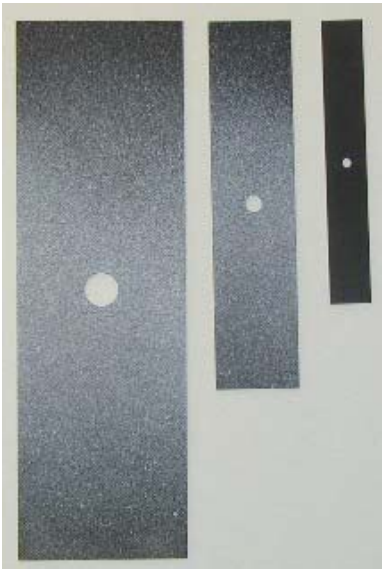

Figure 4.2 Specimens with pattern.

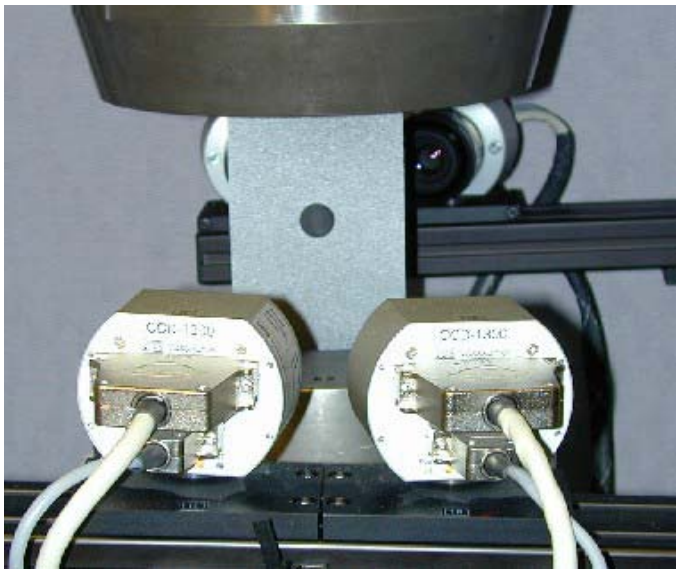

Figure 4.3 Experimental setup with four cameras.

DSP were used for the medium and large specimens, but not for the small ones. Therefore the right specimen in Figure 4.2 has no pattern.

4.3 Data acquisition

During testing of the specimens two methods for logging the strain levels were used: the strain levels for the strain gages were collected continuously and the whole field strains were collected with the DSP equipment at some predetermined load levels.

The strain gages and the load signal from the test machine were connected to a Dewe-Port 2000 portable PC manufactured by Dewetron. Wheatstone bridges and amplifiers were included in the Dewe-Port 2000. The software used for the data acquisition was TestPoint 3.2b. During testing, the strains from the strain gages were logged two times per second, and since each test took about eight minutes to perform that gave about 1000 logged strains per strain gage.

For the data acquisition of the optical measurements a system from GOM (Gesellschaft für Optische Messtechnik) was used. The pictures were taken at some predetermined load levels (steps), about 40 steps per

specimen. As the strain calculations can not be done in real-time they were made after failure of the specimen. Further details of the system can be found in Chapter 5.

4.4 Test procedure

The specimens had been manufactured in three sizes (5, 10 and 20 mm notch and 25, 50 and 100 mm width, respectively) and the tests were performed with stroke (displacement) control, except for the smallest specimens, both in tension and compression. For the medium and large specimens the same test machine was used – a 200 kN servohydraulic MTS 880 machine controlled by Test Star 2, but with different stroke rates, see Table 4.2. For the small specimens a smaller machine had to be used – a manual 100 kN servohydraulic FFA/MTS machine.

Table 4.2 Test machines and stroke rates.

Notch size [mm]	Maximum capacity of the test machine [kN]	Stroke rate [mm/min]
5	100	Manual load control
10	250	0.2
20	250	0.3

DSP was used for all specimens except for the ones with 5 mm notches due to the small dimensions and the manual load control. To verify that the specimen was symmetrically mounted in the test machine and that all equipment was working properly, the mechanical testing was performed in the following way:

First, pictures were taken with the DSP in the unloaded state.

Secondly, a low test load was applied. Strain gages 3 and 4 (see Figure 4.1) were compared at that low load level to verify that the specimen was symmetrically inserted in the test machine. At the same time, pictures were taken with the DSP to check the pattern of the specimen and to compare the strain gage results with the calculated strain from the DSP. After that the specimen was unloaded. Table 4.3 presents the average value of the strain gage with the highest strain level at the test load.

Table 4.3 Strain at test load.

Notch size [mm]	Average maximum strain at the test load [%]	
	Tension	Compression
5	0.05	0.05
10	0.10 [1]	0.06
20	0.13 [2]	0.06

[1]: For T000/10-1 and T000/10-3 the strain at the test load was 0.13 %.
[2]: For T000/20-2 and T020/20-2 the strain at the test load was 0.16 %.

Thirdly, pictures were taken with the DSP at this new unloaded state and the specimen was subsequently loaded to failure with pictures taken continuously. It is the data from the third part of the test that are analyzed in this report.

Anti-buckling supports with circular holes were used for the tests in compression. The purpose of the anti-buckling supports was to prevent buckling, but on the other hand, the holes in the supports had to be large enough to allow measurements with the DSP, see Table 4.4 and Figure 4.4.

Table 4.4 Viewable areas.

Notch size [mm]	Viewable area	
	Tension	Compression
10	Full width (50 mm)	Circle (∅40 mm)
20	Full width (100 mm)	Circle (∅60 mm)

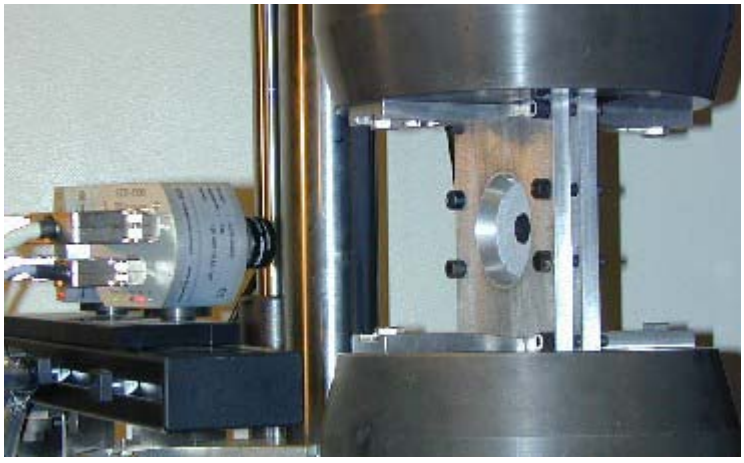

Figure 4.4 Anti-buckling support on a 100 mm width specimen.

To enable the use of cameras on both sides of the specimens with holes, the hole had to be filled to prevent light on one side from dazzling the cameras on the other side. The stiffness of the filling had to be much

lower than the stiffness of the laminate, and therefore soft rubber was used.

4.5 Inclusion tests

The intention with this report was to test the laminate, but the inclusion material was also tested to verify the properties given by the manufacturer in Table 3.5. The inclusion specimens were cut in small rods (approximately 3x4x20 mm^3) from the 20 mm inclusions that had been tested in tension. The inclusion rods were then potted into cylindrical end blocks of steel and tested in compression with perpendicular strain gages. To avoid moments one of the end blocks was supported by a hemispherical bearing. The setup is shown in Figure 4.5.

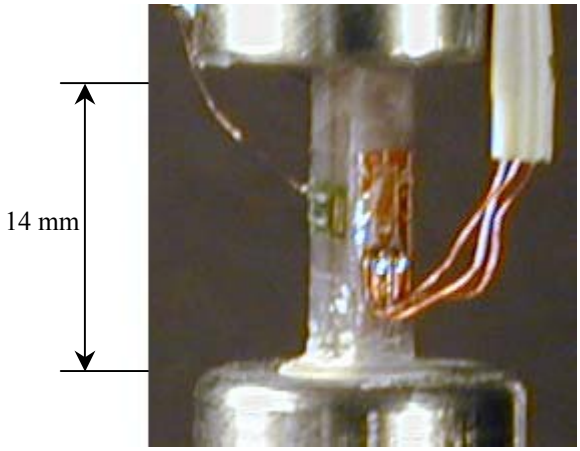

Figure 4.5 Experimental setup for the tests of the inclusion material.

The strain gages were connected to the Dewe-Port 2000 described in Chapter 4.3 and loaded in compression to failure.

5. Optical measurement

The optical measurement technique used for these experiments was DSP – Digital Speckle Photography. DSP is based on the observation of the displacements of a random pattern on the surface of the specimen. By applying ordinary matt white spray paint the random pattern was created. See Figure 4.2.

Before deformation and at some predetermined load levels (steps) pictures are taken with CCD-cameras (CCD = Charged Coupled Device). The images are divided into facets (sub-images) of typically 15x15 pixels and the patterns of the deformed images are compared with the pattern before deformation. As the patterns are compared, the displacements and the strains of each facet can be determined, Melin (1999). Figure 5.1 shows how a part of an image is divided into facets and how they follow the deformation.

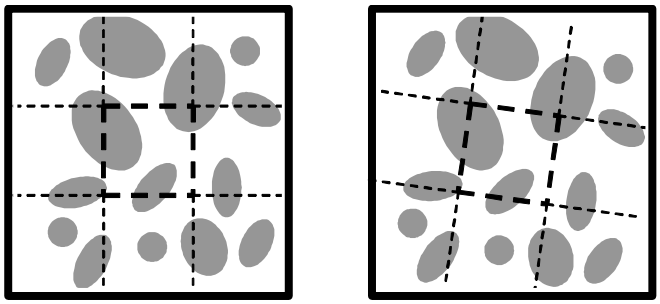

Figure 5.1 Image, divided into sub images, before and after deformation.

2D- or 3D-displacements can be measured using either one or two cameras, respectively. The first two experiments (T000/20-1 and T020/20-1) were performed using only one camera on each side of the specimen. For some reason that gave higher strain levels at the upper part of the specimen than at the lower part. When using two cameras on each side of the specimen this phenomenon disappeared. Therefore 3D-measurements were used for all other experiments.

The equipment for the optical measurements was a system from GOM, mentioned in Chapter 4.3, and included:

- Aramis 4.7 software.
- Four CCD-1300G cameras (CCD = Charged Coupled Device) manufactured by VDS Vosskühler.
- Two different sizes of lenses to the cameras – four with 23 mm lens diameter and two with 50 mm diameter.

A close zoom of the pattern with the 23 mm lens is shown in Figure 5.2a and with the 50 mm lens in 5.2b. Note the distance between the facets and hence, that gives the 50 mm lens higher spatial resolution than the 23 mm lens. The strains (displacements) are calculated at the center of each facet (yellow cross) over an area of 3x3 facets.

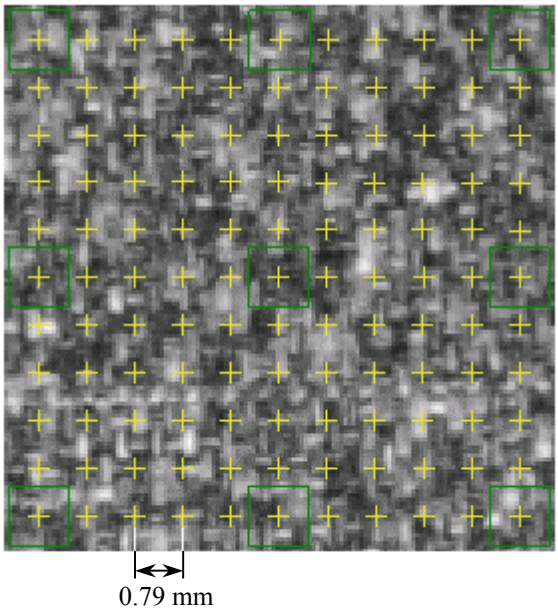

Figure 5.2a Zoom of the pattern, 23 mm lens.

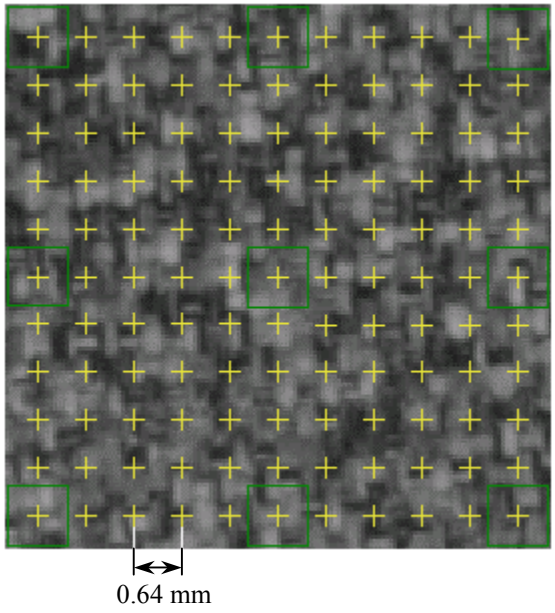

Figure 5.2b Zoom of the pattern, 50 mm lens.

The type of measurement and the cameras used can be found in Table 5.1.

Table 5.1 Type of measurement and lens diameter.

Specimen	Type of measurement	Lens diameter [mm] Front	Back
T000/10-1, 2, 3	3D	50	(*)
T000/20-1	2D	23	23
T000/20-2	3D	23	23
T000/20-3	3D	23	50
T020/20-1	2D	23	23
T020/20-2, 3	3D	23	50
TCUT/10-1, 2, 3	3D	50	(*)
TCUT/20-1, 2, 3	3D	23	50
Compression, all specimens	3D	23	50

(*): No cameras on the back were used.

The DSP presents the results in a color map where the color illustrates different strain levels; see the example in Figure 5.3 where a laminate

with a 20 mm inclusion was tested in tension. (Figure C.1 in Appendix C is the same as Figure 5.3 but with a strain scale.) This way to present results is useful for a quick whole field picture of the strains, for example to determine local strain concentrations.

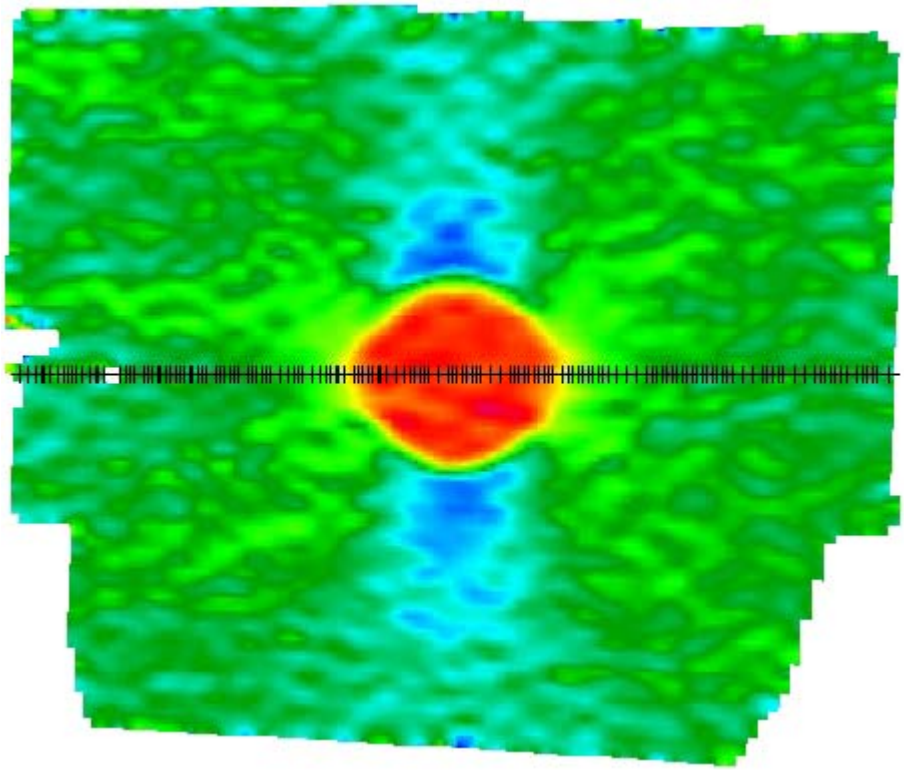

Figure 5.3 Example of results for a tension test presented as a color map of the strain in the loading direction, see Figure C.1 for a strain scale. Specimen T020/20-2. σ^{∞} = 156 MPa. (DSP picture taken with 23 mm lens.)

For the analysis in this report more detailed information about the strains was wanted and a line was drawn through the center of the notch, note the black line through the inclusion in Figure 5.3. The strain at each facet on this line was then exported to a text file and plotted; see the example in Figure 5.4.

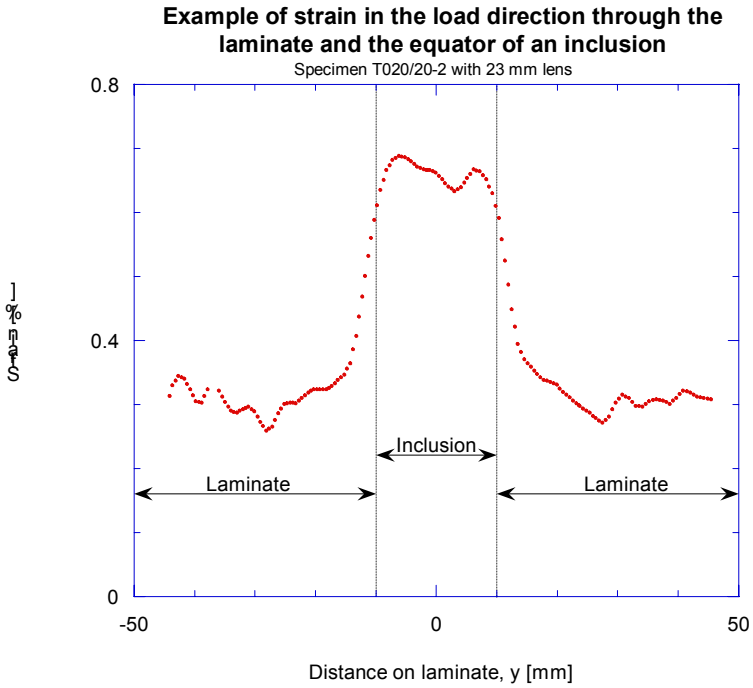

Figure 5.4 Example of results for a tension test presented as a plot of the strain in the loading direction, on the line in Figure 5.3, through the laminate and the equator of the inclusion. ε_{ff} = 0.31 %, σ^{∞} = 156 MPa.

If no facets exist on the line mentioned above, then the Aramis software interpolates facets on the line.

The average values of the strains on either side of the specimen were used for the analysis of experiments with cameras on both sides of the specimen. Since the pictures were taken at predetermined load levels and the experiments were destructible, it was difficult to get pictures close to failure, and thereby measurements can not be done immediately before failure of the specimen.

6. Results

6.1 Overview

To find the failure strains and stresses of the unnotched specimens and to determine whether the laminates were linear elastic or not, six unnotched specimens were tested, three in tension and three in compression. The stress was measured with the load signal, the strains were measured with two strain gages per specimen and their averages in tension and compression are presented in Figure 6.1.

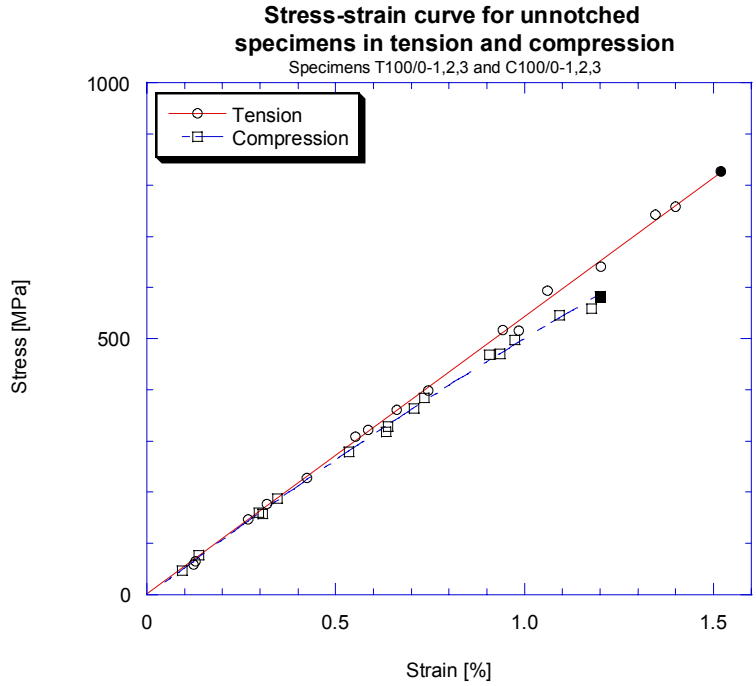

Figure 6.1 Stress-strain curve for unnotched specimens in tension and compression.

As seen in the figure above the behavior of the laminate is linear elastic in tension, but only linear elastic up to about 0.6 % strain in compression. The average properties for the unnotched specimens are presented in Table 6.1. Failure data for all specimens can be found in Appendix A and Appendix B.

Table 6.1 Properties of unnotched specimens in tension and compression.

Loading	Failure strain [%]	Stress at failure [MPa]	Secant modulus [GPa]
Tension	1.52	828	54.3
Compression	1.20	583	52.5 (*)

(*): Linear elastic region.

The behavior of the tension tests of specimens with a soft inclusion was undesired – the inclusion debonded from the laminate at a stress level of about 50 % of the failure stress of the entire laminate. See Figure 6.2a and 6.2b.

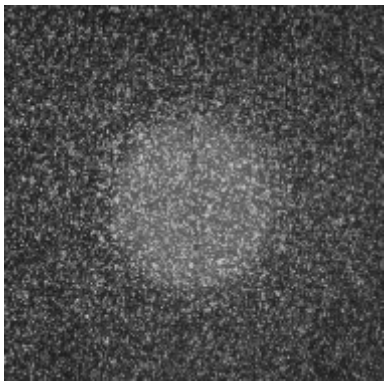

Figure 6.2a Inclusion and laminate bonded together, $\sigma \leq \sigma_{low}$.

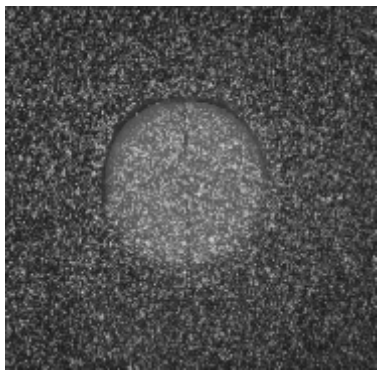

Figure 6.2b Inclusion debonded from the laminate, $\sigma > \sigma_{low}$.

Three specimens were tested in tension with a soft inclusion and all of them showed this behavior. To get comparable results for all specimens with all types of notches the results are presented at the lowest level, σ_{low}, when laminate and inclusion still are bonded together. It was specimen 2 in tension (T020/20-2) that settled σ_{low} to be approximately 160 MPa. At σ_{low} the far-field strain is about 0.3 % and the strain in the inclusion about 0.7 %.

Since the inclusions from the specimens tested in tension (T020/20-1,2,3) were intact after testing of the laminate they were cut to small specimens (3x4x20 mm^3) and tested in compression to determine Young's modulus and Poisson's ratio. The weighted averages from the tests are shown in Figure 6.3.

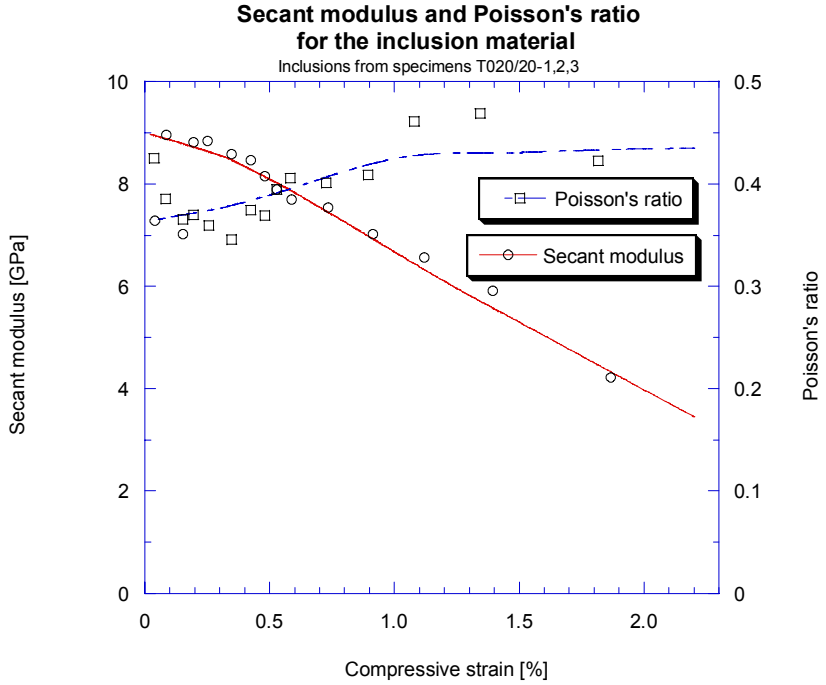

Figure 6.3 Secant modulus and Poisson's ratio for the inclusions from specimens T020/20-1,2,3.

As seen, the inclusion properties are not linear elastic. For 0.7 % compressive strain the secant modulus is 7.4 GPa and Poisson's ratio is 0.41, for 1.5 % compressive strain the secant modulus is 5.0 GPa and Poisson's ratio is 0.43 %, which are fairly different from the properties in Table 3.5.

After testing of the laminate and the inclusion, the following data were used for the analysis:

Table 6.2 Data for the specimens used in the analysis.

	Stress level	Young's modulus	Poisson's ratio
Laminate	All stress levels	E_{lam} = 52.5 GPa	ν_{lam} = 0.31
Inclusion	Low, σ_{low} ($\varepsilon \approx 0.7$ %)	E_{inc} = 7.4 GPa	ν_{inc} = 0.41
	High ($\varepsilon \approx 1.5$ %)	E_{inc} = 5.0 GPa	ν_{inc} = 0.43

The theoretical solutions from Chapter 2 are based on the data in Table 6.2 and gives:

Table 6.3 Predicted results for plane stress conditions.

Notch type		
Stress concentration factor	Hole	$K_{T,H}^{\infty} = 3.0$
	Inclusion	Low load: $K_{T,I}^{\infty} = 2.3$ High load: $K_{T,I}^{\infty} = 2.5$
Finite width correction factor	Hole	$Y_H = 1.05$
	Inclusion	$Y_I = 1.03$

The optical measurements provided the strains at all facets over the entire plate, $\varepsilon = \varepsilon(x,y)$, but for this analysis the strains in the loading direction at the equator of the hole, $\varepsilon_x = \varepsilon_x(0,y)$, were of major importance. To compare the strain distribution at the equator for different notch types the average strain distribution for all specimens of the same type was used. According to Chapter 5 the strains are calculated at the facets, but the locations of the facets are, for example, depending on the cameras and the position of the specimen in the loading machine. Hence, the coordinates of the facets were not identical for the specimens. If the locations of the facets had been the same the average strain simply had been the sum of the strains at the facet divided with the number of used specimens. However, the strain (stress) distribution was not linear, but distributed as a fourth-degree-polynomial (see Chapter 2), which made it complicated to obtain the correct average strain. Instead the average strain distribution was calculated in the following way: all strains (front, back, left and right side, in the order of 50 facets per side) from the optical measurements were put together in the same plot and a curve fit with the Levenberg-Marquardt algorithm was done as an approximation of all strains. An example is shown in Figure 6.4.

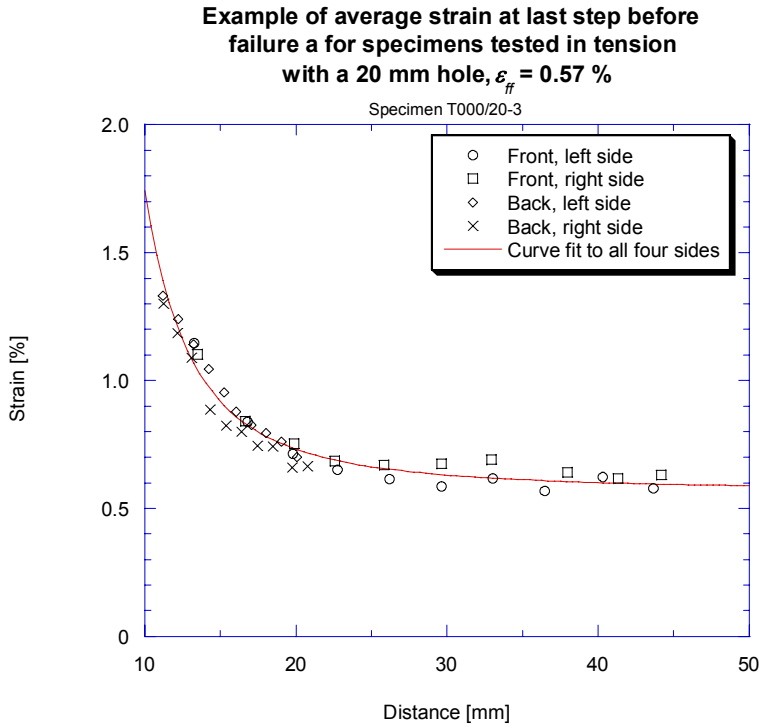

Figure 6.4 Example of average strain.

This method made it easy to calculate the average strain distribution for all specimens of the same type – the strain at the facets were put in the same plot and a curve fit was done to all 12 sides (if three tests of the same type were done). All curves are based on at least 100 data points and only a fraction of these points are shown in the graphs.

A curve fit of the strain over the equator of the hole / inclusion / cut fibers was done to determine the far field strain, ε_{ff}, with the optical measurements. Considering Equation (2.16) the chosen equation for the curve fit was a fourth-degree polynomial:

$$\varepsilon_x(0,y) = \varepsilon_{ff}\frac{1}{2}\left(b_1 + b_2\left(\frac{R}{y}\right)^2 + b_3\left(\frac{R}{y}\right)^4\right)$$

where R is half the notch size ($R = D / 2$) and b_i, $i = 1,2,3$ are constants.

Clearly the far field strain is ε_{ff}, if $b_1 = 2$, and the strain in the laminate at the notch, $y = R$, is $\varepsilon_{local} = \varepsilon_{ff}(b_1 + b_2 + b_3) / 2$.

The measured strain concentration factor for the finite width specimen is $K_{\varepsilon T} = \varepsilon_{local} / \varepsilon_{ff}$. To transform $K_{\varepsilon T}$ to be valid for infinite specimens it is assumed that Equation (2.18) also is valid for strain concentration factor:

$$K_{\varepsilon,T}^{\infty} = \frac{K_{\varepsilon,T}}{Y}$$

where the finite width correction factors can be found in Table 6.3.

6.2 Tension

The normalized strain in tension at σ_{low} for specimens with a 20 mm notch is presented in Figure 6.5.

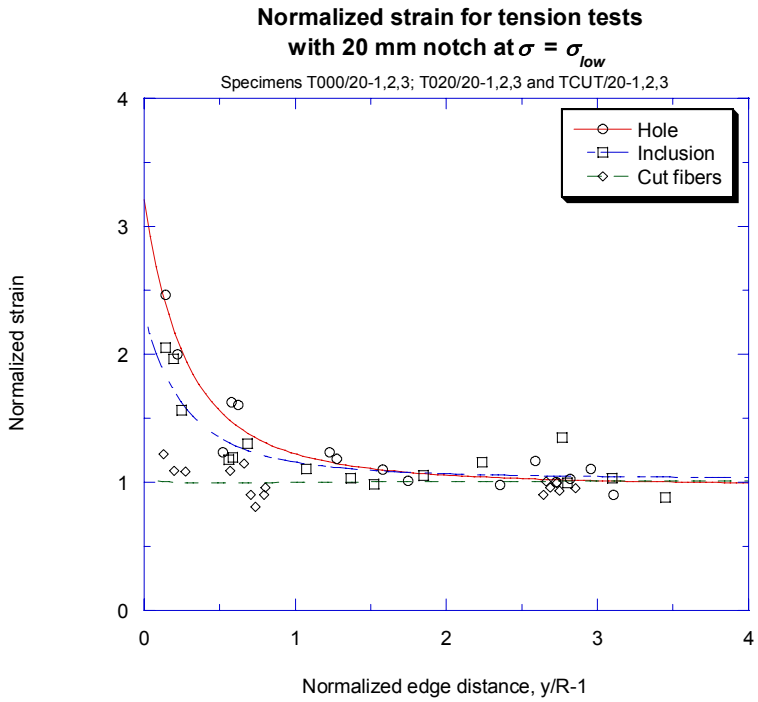

Figure 6.5 Normalized strain in tension with three types of 20 mm notches at σ_{low}, averages for all specimens.

The strain distributions are plotted for two different hole diameters and load levels in Figure 6.6. The lower load is σ_{low} and the higher load is the last step in DSP before visible damage.

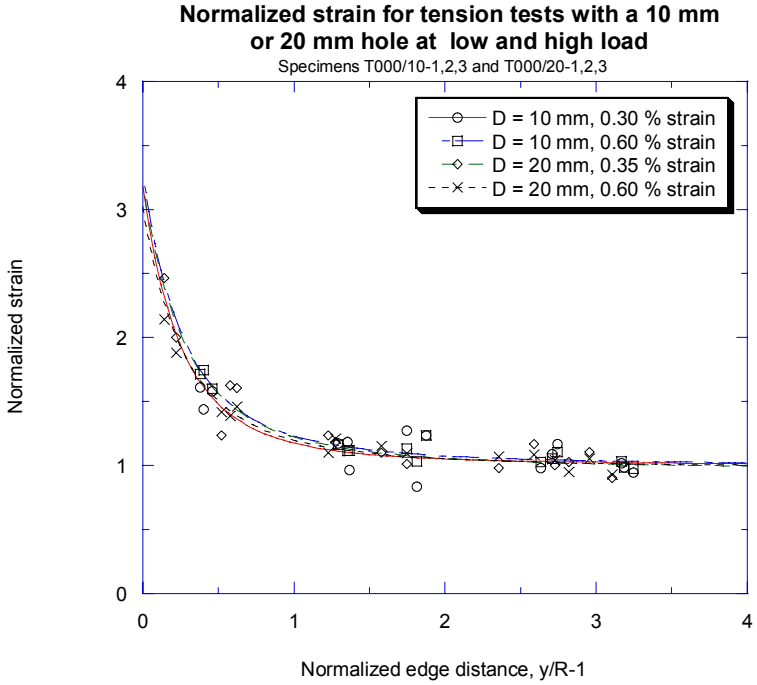

Figure 6.6 Normalized strain for specimens with holes in tension with different diameters and load levels, averages for all specimens.

The strain concentration factors in Figures 6.5 and 6.6 are:

Table 6.4 Measured strain concentration factors for specimens in tension.

Notch diameter [mm]		Low load		High load	
		Finite plate	Infinite plate	Finite plate	Infinite plate
Hole	10	3.2	3.0	3.3	3.1
	20	3.2	3.0	3.0	2.9
Inclusion	20	2.3	2.2	-	-
Cut fibers	20	1.0	-	-	-

The average strain concentration factor for all finite width specimens with holes at different load levels is $K_{\varepsilon,TH} = 3.2$ which gives $K^{\infty}_{\varepsilon,TH} = 3.0$ for infinite plates. This strain concentration factor, for the high load, gives strain levels over 1.9 % near the hole, which is 25 % higher than the unnotched strength, and a local damaged area would be expected.

The strain concentration factor for specimens with cut fibers increases with the load. One reason is the opening of the crack, which gives the laminate larger deformations near the crack tip than in the far field.

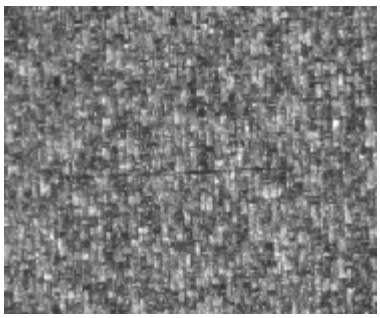

Figure 6.7a Cut fibers (D = 10 mm, specimen 3) in tension at σ = 256 MPa, ε = 0.46 %.

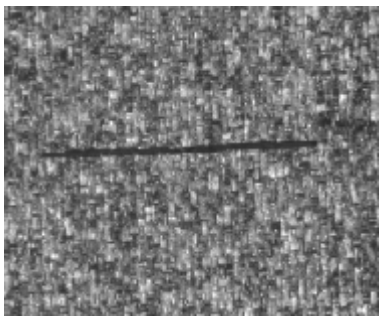

Figure 6.7b Cut fibers (D = 10 mm, specimen 3) in tension at σ = 412 MPa, ε = 0.72 %.

Figure 6.7 shows specimen 3 with 10 mm cut fibers (TCUT/10-3) but this behavior is consistent for all specimens with cut fibers in tension. The normalized strain ahead of the crack for these two stress levels (and a stress level between them) is shown in Figure 6.8. The failure stress of this specimen was 418 MPa.

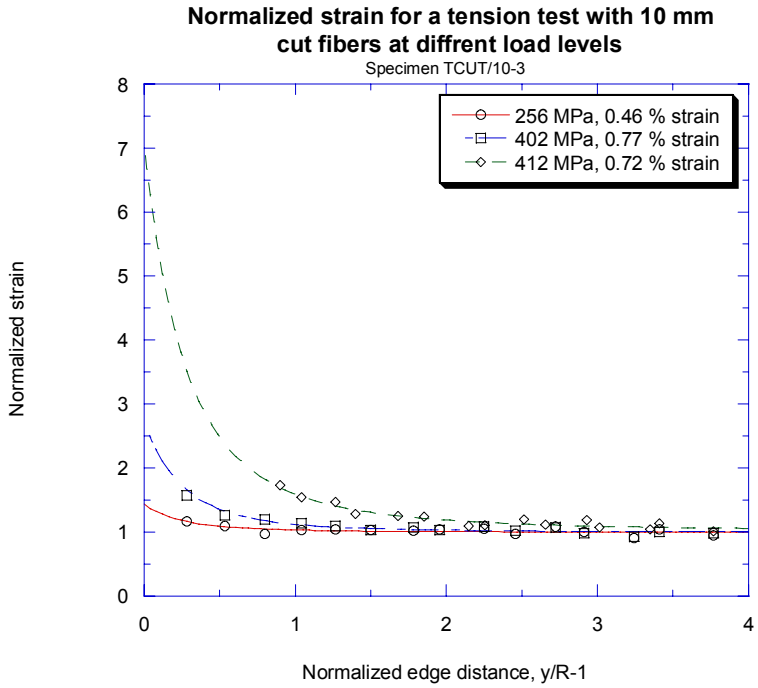

Figure 6.8 Normalized strain at different stress levels for specimen 3 with 10 mm cut fibers in tension.

At the stress level of 412 MPa, the far field strain has decreased and points are missing in the interval $0 \le y/R\text{-}1 < 0.75$ due to the deformed surface close to the notch tip. One explanation to the decrease in strain

could be that the DSP make measurements on the surface. If a surface layer of a laminate is not completely bonded to the next layer then the accuracy of the strain measurements decreases. The stress, on the other hand, is measured through the loading machine and debonding in the notched section has no effect on the stress measurements. Consequently – higher load gives larger strain concentration.

6.3 Compression

The normalized strain in compression at σ_{low} for specimens with a 20 mm notch is presented in Figure 6.9.

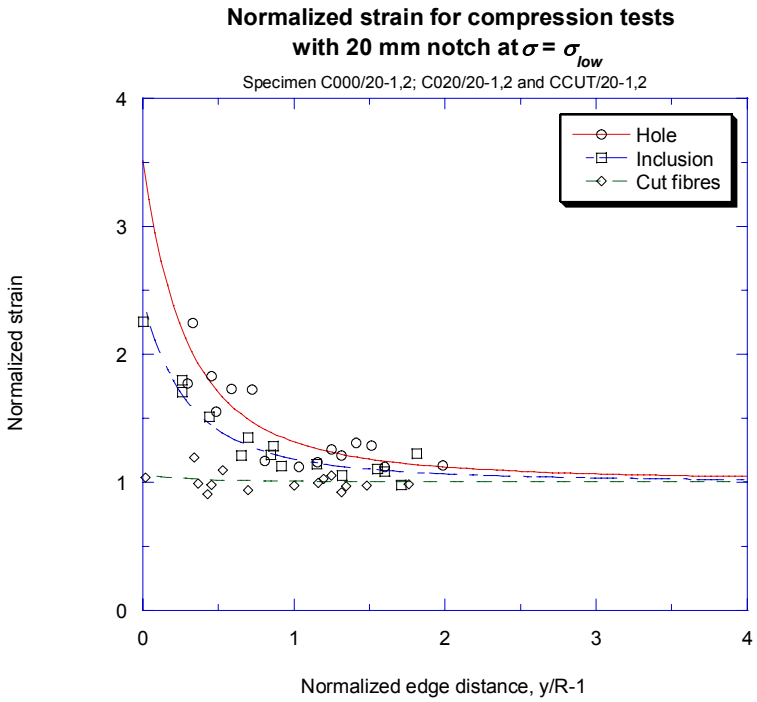

Figure 6.9 Normalized strain in compression with three types of 20 mm notches at σ_{low}, averages for all specimens.

The strain distributions at two different load levels are plotted in Figure 6.10 and Figure 6.11 for hole and inclusion, respectively. The lower load is σ_{low} and the higher load is the last step in DSP before visible damage.

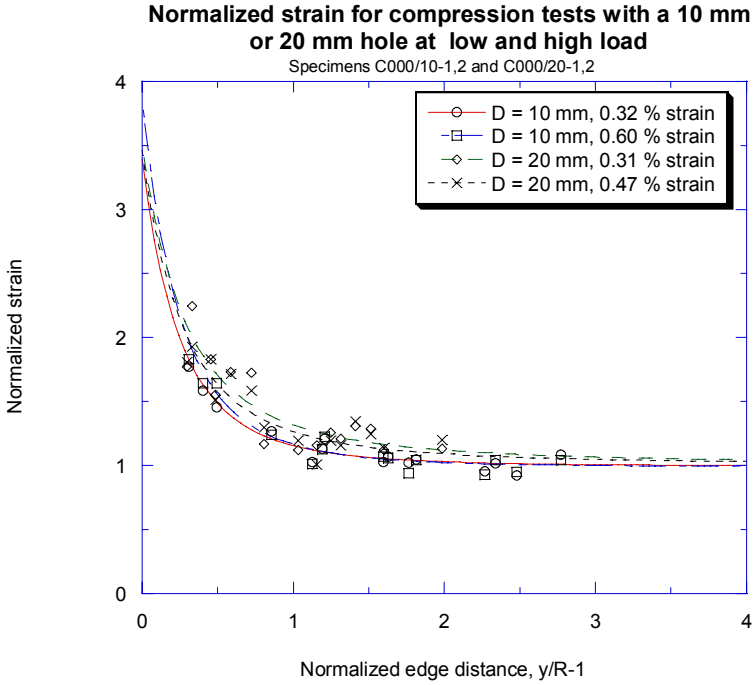

Figure 6.10 Normalized strain for specimens with holes in compression with different diameters and load levels, averages for all specimens.

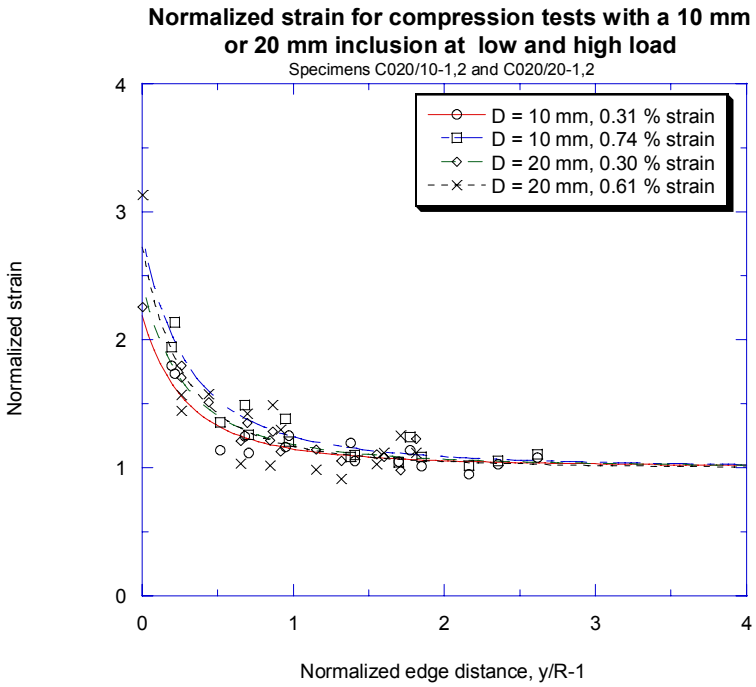

Figure 6.11 Normalized strain for specimens with inclusion in compression with different diameters and load levels, averages for all specimens.

The strain concentration factors in Figures 6.9, 6.10 and 6.11 are:

Table 6.5 Measured strain concentration factors for specimens in compression.

Notch diameter [mm]		Low load		High load	
		Finite plate	Infinite plate	Finite plate	Infinite plate
Hole	10	3.4	3.2	3.9	3.7
	20	3.5	3.3	3.4	3.2
Inclusion	10	2.2	2.1	2.8	2.7
	20	2.4	2.3	2.7	2.6
Cut fibers	20	1.0	-	-	-

For different load levels the average strain concentration factor for all finite width specimens with holes is $K_{\varepsilon TH} = 3.5$ which gives $K^{\infty}_{\varepsilon,TH} = 3.3$ for infinite plates. For specimens with inclusion the strain concentration factors are $K_{\varepsilon TI} = 2.5$ and $K^{\infty}_{\varepsilon,TI} = 2.4$ for finite and infinite plates, respectively.

As earlier mentioned, the average strain values of the front- and backside were used for the analysis. Though anti-buckling supports were used in compression an observable buckling occurred for the large specimens. Since the thickness is the same, the large specimens have a lower buckling strain than the smaller ones. The buckling gives higher strain levels on one side of the surface than on the other, due to the superposition of negative membrane strain (equal on both sides) and bending strain (negative on the “inner” side). See Figure 6.12.

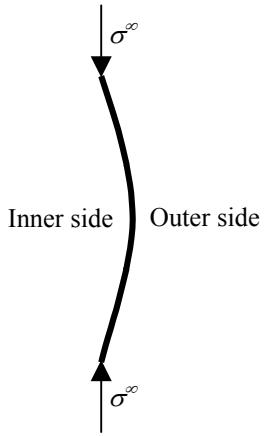

Figure 6.12 Definition of inner and outer side for the compression tests.

6.4 Failure criteria

Based on the failure stress and the properties of the inclusion at high stress levels the characteristic lengths d_0^σ and a_0^σ can be determined by using Equation (2.31) and Equation (2.32). The characteristic lengths may either be determined to satisfy the equations exactly for a given diameter, or by selecting a fixed value which gives the best curve fit approximation for all diameters. The curve fit approximations are shown in Figure 6.13. Note that the average stress criterion gives a slightly better fit than the point stress criterion.

Table 6.6 Characteristic lengths based on failure stress.

Notch type	D [mm]	PSC: d_0^σ [mm]		ASC: a_0^σ [mm]	
		Tension	Compression	Tension	Compression
Hole	5	0.61	1.08	1.49	3.03
	10	0.95	1.75	2.20	4.63
	20	0.99	2.23	2.15	5.32
	Curve fit	**0.71**	**1.39**	**1.74**	**3.94**
Inclusion	5		2.22		8.56
	10		2.34		6.77
	20		2.83		7.08
	Curve fit		**2.41**		**7.32**

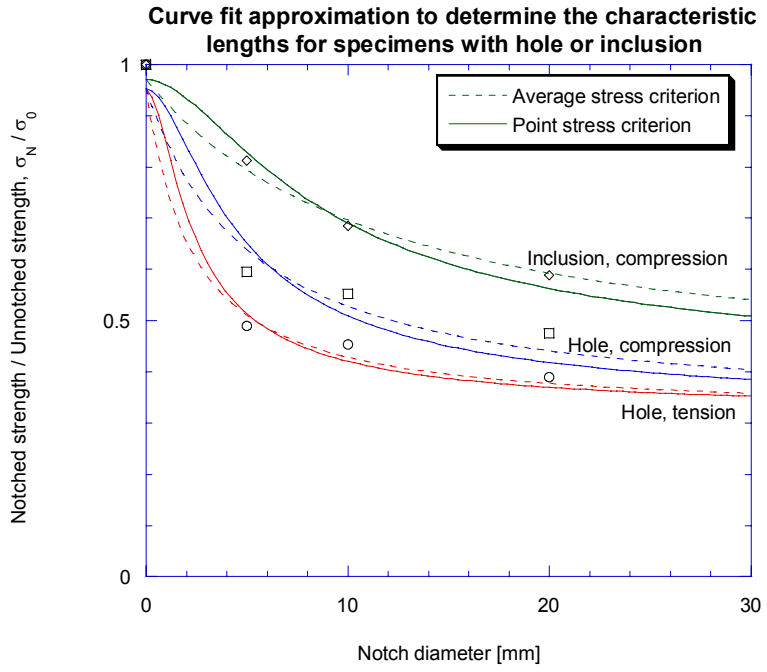

Figure 6.13 Curve fit approximation to determine the characteristic length.

7. Discussion

7.1 Evaluation of data

As mentioned in Chapter 5: “The strains are calculated at the center of each facet over an area of 3x3 facets”. Looking at Figure 7.1 one realizes that the strain in the facet represented as a white circle is calculated using the strains at all facets in the white 3x3 facet square.

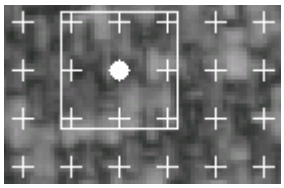

Figure 7.1 Area for strain calculations.

What happens when a crack or a hole propagates through this white 3x3-square? See Figure 7.2.

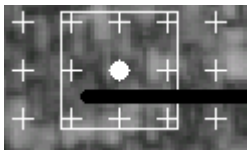

Figure 7.2a Area for strain calculations with a crack.

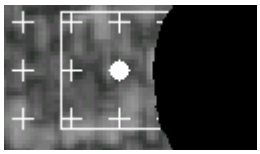

Figure 7.2b Area for strain calculations with a hole.

In Figure 7.2a all facets can be used for calculation, but the strains in the circle-facet are calculated using facets on the opposite side of the crack. The result is fictitious – often with strain levels over 4 % – which are irrelevant for further evaluation, see Figure 7.3. In Figure 7.2b the strains in the circle-facet are calculated over a 3x2-area since three facets are inside the hole. The strains in the circle-facet can be used, but due to the possibility that the strains are calculated at a (fictitious) point a short distance to the left, instead of at the exact position of the facet, the strains in these facets have been ignored.

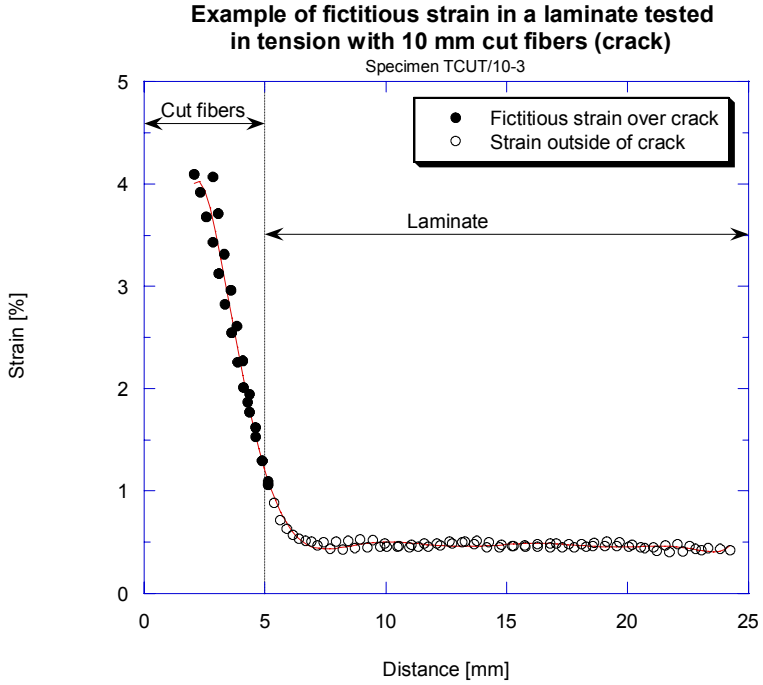

Figure 7.3 Fictitious strain in laminate with crack (cut fibers).

7.2 Strain distribution

In this report it was assumed that the finite width correction factor derived for stress (Chapter 2.2) also is valid for strain. Linear elastic theory was also assumed, although Figure 6.3 indicates plastic behavior.

The two normal and one shear stress are, according to Equation (2.8), constant in the inclusion for orthotropic laminates. To verify that, the von Mises strain in the inclusion and the neighboring laminate is presented in Figure 7.4a and D.1. The von Mises strain on the equator of the inclusion (and neighboring laminate) is illustrated with a black line and shown in Figure 7.4b.

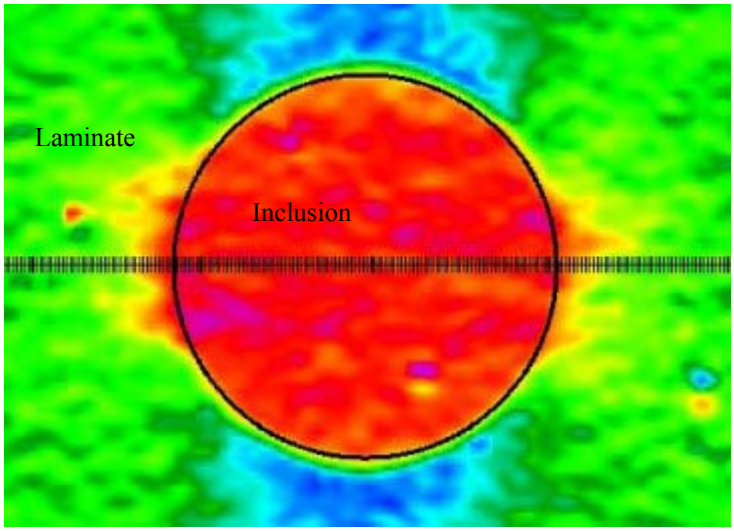

Figure 7.4a von Mises strain distribution in the inclusion (D = 20 mm) and neighboring laminate. (DSP picture taken with 50 mm lens.)

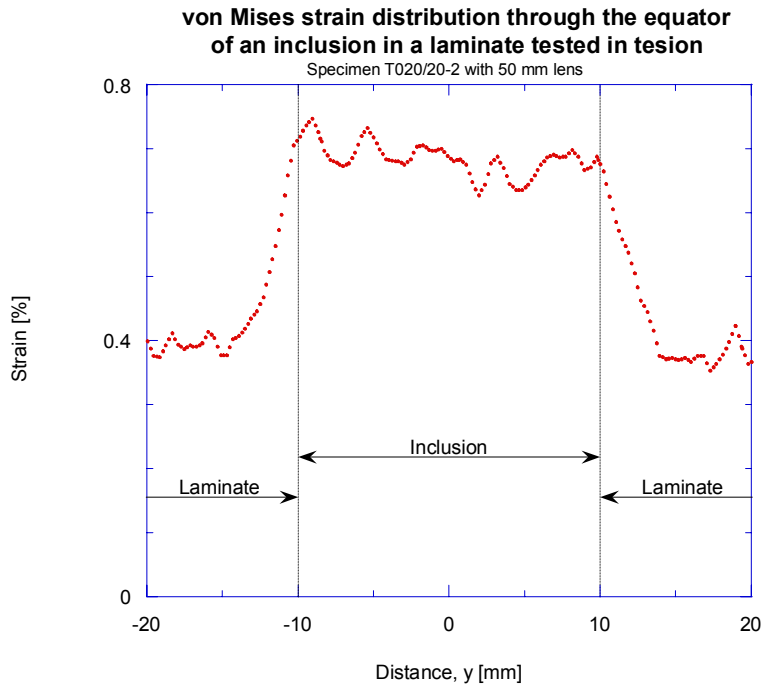

Figure 7.4b von Mises strain along the equator of the inclusion.

As seen in the figures the strain is fairly constant in the inclusion. Figure 5.3, 5.4 and Figure 7.4 are based on the same specimen and load level, T020/20-2 at $\sigma_{low} = 156$ MPa, but at different sides of the specimen. Figure 7.4 gives higher resolution due to its 50 mm lenses. By averaging the strain in the loading direction from both sides the following results are found:

$$\left.\begin{aligned}\varepsilon_{inclusion} &= 0.68\,\% \\ \varepsilon_{ff} &= 0.31\,\%\end{aligned}\right\} \Rightarrow \frac{\varepsilon_{inclusion}}{\varepsilon_{ff}} = 2.2$$

which is about 8 % lower than the strain concentration factor for all specimens with 20 mm inclusion tested in compression, see Table 6.5.

7.3 Stress distribution

There are two ways to calculate the stress distribution around an inclusion in this report: Xiong's or Goodier's solutions – Equations (2.5) or (2.11), respectively. Xiong's solution was derived for anisotropic plates under plane stress, while Goodier's solution was derived for isotropic plates under plain strain. The constants in Goodier's original plane strain solution are given in Equation (2.12). The corresponding constants for plane stress conditions may be obtained by a proper transformation and are given in Equation (2.14). It was also verified that Xiong's solution and Goodier's solution, transformed to plane stress, yield identical results. A comparison of the plane strain and plane stress solutions is shown in Figure 7.5 where the solution for a hole in an isotropic plate, Equation (2.4), is shown as a reference.

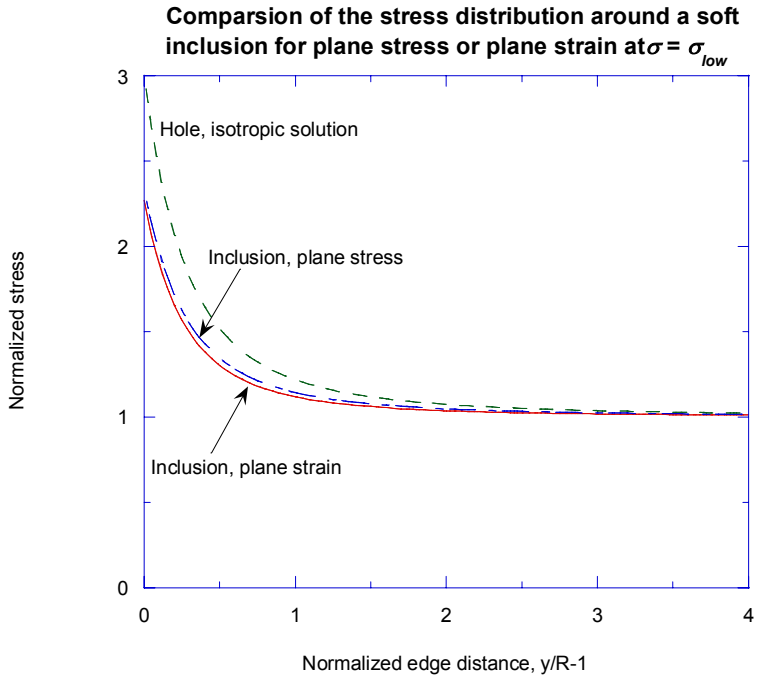

Figure 7.5 Comparison of plane stress and plane strain solutions for the stress distribution in the loading direction.

As seen in the figure, the plane strain solution gives only a slightly lower normalized stress than the solution for plane stress. The constants in Equations (2.12) and (2.14) are:

Table 7.1 Constants used to express the stress and strain distributions as fourth-degree polynomials.

Constant	Hole	Inclusion ($\varepsilon_z = 0$)	Inclusion ($\sigma_z = 0$)	
		Low load	Low load	High load
c_1	2.00	2.00	2.00	2.00
c_2	1.00	0.42	0.64	0.73
c_3	3.00	2.12	2.05	2.32

The predicted strain concentration factors are calculated using Equation (2.16) at $y = R$. Note that the predicted $K^{\infty}_{\varepsilon,TH} = K^{\infty}_{TH}$ for specimens with a hole since $\sigma^{\infty}_{y}(0,R) = 0$

Table 7.2 Predicted and measured strain concentration factors.

	Notch type	Hole		Inclusion	
	Load level	Low	High	Low	High
Predicted $K^{\infty}_{\varepsilon,T}$		3.0	3.0	2.3	2.5
Measured $K^{\infty}_{\varepsilon,T}$	Tension	3.0	3.0	2.2	-
	Compression	3.3	3.5	2.2	2.7

The measured average strain distribution for tension and compression tests at σ_{low} may now be compared with the predicted strain distribution, Equation (2.16), and the predicted stress distribution, Equation (2.11a), at plane stress conditions in an infinite plate, see Figure 7.6a and 7.6b for specimens with hole and inclusion, respectively.

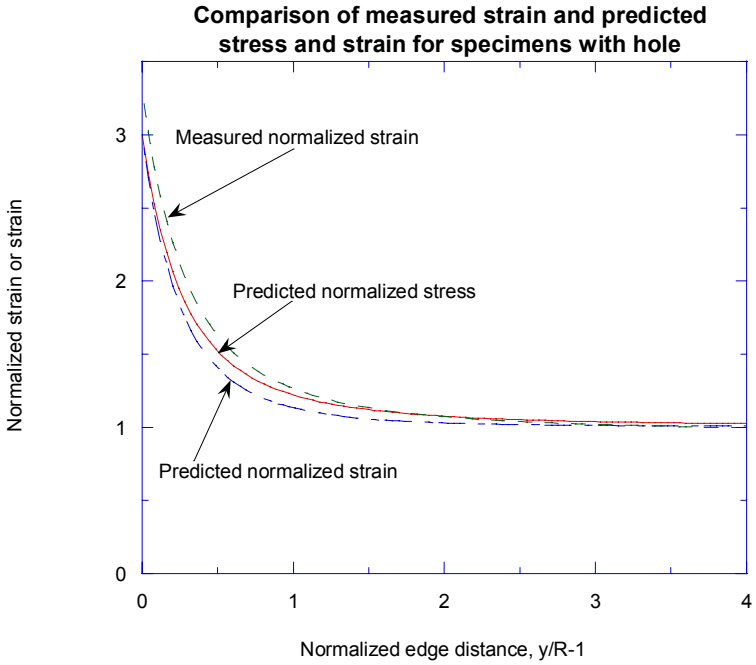

Figure 7.6a Comparison of normalized strain distribution and normalized stress distribution for specimens with hole.

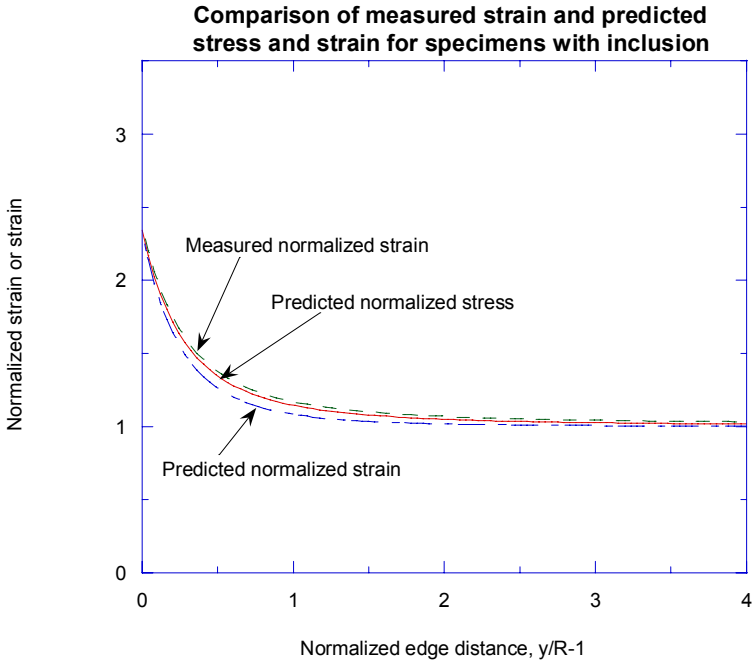

Figure 7.6b Comparison of normalized strain distribution and normalized stress distribution for specimens with inclusion.

The figures show that the measured normalized strain is higher than the predicted normalized strain. This is what would be expected, since the corrections for finite width are neglected in Figure 7.6.

In this study only the strain in the loading direction is considered. To improve the analysis the strain perpendicular to the load should be included in the comparison of normalized stress and strain.

7.4 Finite width correction factor

Gillespie and Carlsson (1988) proposed an expression that corrects the entire stress distribution due to finite width, Equation (2.23). That expression was verified in the reference by finite element experiments for specimens with hole. For future work, Equation (2.23) should be verified for specimens with soft inclusion, for example by finite element calculations.

Dost et al. (1988) proposed an approximate expression of the finite width correction factor for orthotropic laminates with inclusion, Equation (2.28), which is much less complicated than the one derived by Xiong (1994), Equation (2.26). For the quasi-isotropic specimens in this report the difference between Equation (2.26) and (2.28) is only in the order of 1 %. Therefore, the expression of the finite width correction factor in Equation (2.28) works as a good approximation. Furthermore, the expression derived by Xiong (1994) contains singularities for quasi-isotropic laminates, which makes it even more complicated.

7.5 Failure criteria

The characteristic lengths for point stress criterion (PSC) and average stress criterion (ASC) based on the failure stress (superscript σ) decrease with smaller notch size as shown in Table 6.6. This can be explained by the 3D-effects near the hole that increase the stress level in the laminate. All laminates had a load bearing thickness of about 3 mm and a specimen width / notch size ratio of 5. To keep the influence of 3D-effects constant, the thickness of the laminate should have been scaled in the same way as the notch size and the specimen width.

Based on the strain distribution from the optical measurement at the last step before visible damage and the failure strain of the unnotched specimens, the following characteristic lengths, d_0^{ε} and a_0^{ε}, for PSC and ASC, respectively, are found:

Table 7.3 Characteristic lengths based on the strain distributions in the optical measurement.

Notch type	D [mm]	PSC: d_0^ε [mm]		ASC: a_0^ε [mm]	
		Tension	Compression	Tension	Compression
Hole	10	0.46	1.47	0.99	3.81
	20	0.80	1.33	1.71	2.96
	Curve fit	**0.47**	**1.41**	**1.02**	**3.45**
Inclusion	10		2.06		5.51
	20		1.89		4.38
	Curve fit		**1.93**		**4.89**

Note that no DSP was used for the specimens with 5 mm notch and that the curve fit approximation of the characteristic lengths is made in the same way as in Chapter 6.4.

The method used to find the characteristic lengths in Table 7.3 is in some literature, for example in Tan (1994), denoted as “point strain criterion” and “average strain criterion”.

To compare the characteristic lengths based on failure stress (d_0^σ and a_0^σ) with the ones based on the strain distribution from the DSP (d_0^ε and a_0^ε), the specimens with 5 mm notch are removed from Table 6.6 and new curve fit approximations are made:

Table 7.4 Characteristic lengths for specimens with 10 mm or 20 mm hole or inclusion.

Notch and loading	PSC		ASC	
	d_0^σ	d_0^ε	a_0^σ	a_0^ε
Hole, tension	0.96	0.47	2.19	1.02
Hole, compression	1.89	1.41	4.87	3.45
Inclusion, compression	2.51	1.93	6.91	4.89

It would be expected to find the characteristic lengths calculated from the strain distribution to be shorter than the ones based on the failure stress since they are evaluated at a lower stress level (about 9 %) due to the limitations in the DSP. As shown in Table 7.4, $\left(d_0^\varepsilon, a_0^\varepsilon\right) < \left(d_0^\sigma, a_0^\sigma\right)$ for all notch types and load configurations.

8. Summary and conclusions

Tension and compression tests were performed on quasi-isotropic laminates with three different types of artificial impact damage (notches) – hole, soft inclusion and cut fibers. The laminates had been manufactured in three different sizes where all dimensions except the thickness were scaled.

The tests showed undesired, but expected, behavior for the tension tests of the laminates with inclusion – the inclusions debonded from the laminate at a stress level of about 50 % of the failure stress. Hence, the results from these tests were only valid up to the debonding stress.

The strain field around the notches was measured with DSP (Digital Speckle Photography). The measurements showed very high strain concentrations in a small region close to the notch edge for the tension tests of specimens with cut fibers, but barely any strain concentrations for the compressive tests of the same type of notch. Due to the problem to resolute this small region with the DSP the tests with cut fibers are not analyzed in detail in this paper.

For the specimens with holes or inclusions the strain field was measured and compared with analytical expressions for the stress and stress distributions. It was further assumed that the finite width correction factor derived for stress also was valid for strain. There was barely any difference between the measured strain concentration factor and the theoretical strain concentration factor for the tension tests. For the compression tests the strain concentration factor showed to be about 5 % higher than predicted. One explanation may be that the inclusion showed a plastic behavior at fairly low strain levels.

The characteristic lengths for the point stress criterion (PSC) and the average stress criterion (ASC) were determined in two ways: by the failure stress in the laminate and by the strain distribution on the face of the laminate before the first visible damage, approximately at 9 % lower applied stress than the failure stress. It is commonly assumed that the characteristic length is a material property independent of load case, notch type and notch size. However, due to the different fracture mechanisms for tension and compression failure, it is expected to find different characteristic lengths in tension and compression. The characteristic lengths for compressive failure in specimens with hole were in this study found to be approximately two to three times larger than the corresponding length for tensile failure. This study even showed

a notch size dependency – smaller notch sizes gave smaller characteristic lengths. The difference in the characteristic lengths indicates different fracture mechanisms for holes and inclusions. This study showed that the average stress criterion gives a slightly better fit than the point stress criterion, which also has been observed in other studies, Tan (1994). The conclusion that can be drawn is: if the point stress or average stress criterion are used the characteristic lengths need to be adjusted for each notch type and load case.

To improve the study in this report the following modifications should be done:

- Use optical equipment that can resolute the small region close to the notch edge with higher accuracy.
- Improve the inclusion material to bond to the laminate for tension tests and be elastic for higher strain levels.
- Scale the thickness of the laminate in the same way as the notch size is scaled by the specimen width.
- Perform more tests with different notch sizes to determine the notch dependency of the failure criteria.
- Improve the theoretical solutions for the stress distribution and the failure criteria to include 3D-effects close to the notch edge.
- Evaluate the fracture by fractography.

9. References

Abrate, S. 1991. "Impact on laminated composite materials", *Applied Mechanics Reviews*, **44** (4) 155-190.

Awerbuch, A. and Madhukar, M.S. 1985. "Notched strength of composite laminates: predictions and experiments – a review", *Journal of Reinforced Plastics and Composites*, **4** (1) 3-159.

Dost, E.F., Ilcewicz, L.B. and Gosse, J.H. 1988. "Sublaminate stability based modeling of impact-damaged composite laminates", *Proceedings of the 3rd Technical Conference of American Society for Composites*, Seattle, USA. 354-363.

Fung, Y.C. 1965. "*Foundations of solid mechanics*", Prentice-Hall, New Jersey, USA.

Gillespie, J.W., Jr. and Carlsson, L.A. 1988. "Influence of finite width on notched laminate strength predictions", *Composites Science and Technology*, **32** (1) 15-30.

Goodier, J.N. 1933. "Concentration of stress around spherical and cylindrical inclusions and flaws", *Transactions of the ASME*, **55** (7) 39-44.

Konish, H.J. and Whitney, J.M. 1975. "Approximate stresses in an orthotropic plate containing a circular hole", *Journal of Composite Materials*, **9** (2) 157-166.

Lekhnitskii, S.G. 1968, "*Anisotropic plates*", Gordon and Breach, New York, USA.

Melin, L.G. 1999. "Optical whole field measurement techniques for mechanical testing – a review", *FFA TN 1999-35*, The Aeronautical Research Institute of Sweden, Bromma, Sweden.

Nuismer, R.J. and Whitney, J.M. 1975. "Uniaxial failure of composite laminates containing stress concentrations" *Fracture Mechanics of Composites*, ASTM STP 593, 117-142.

Olsson, R. 1999. "A Review of impact experiments at FFA during 1986 to 1998", *FFA TN 1999-08*. The Aeronautical Research Institute of Sweden, Bromma, Sweden.

Olsson, R. 2000. "Large mass impact tests on rectangular composite plates with various layups", *FFA TN 2000-01*, The Aeronautical Research Institute of Sweden, Bromma, Sweden.

Sjögren, A. 1999. “Fractographic characterization of impact damage in carbon fiber/epoxy laminates”, *FFA TN 1999-17*, The Aeronautical Research Institute of Sweden, Bromma, Sweden.

Sjögren, A. 2001. “Manufacturing of carbon fibre/epoxy laminates with artificial damage”, *CR01-075*, Sicomp AB, Mölndal, Sweden.

Sjögren, A., Krasnikovs, A. and Varna, J. 2001. ”Experimental determination of elastic properties of impact damage in carbon fibre/epoxy laminates”, *Composites Part A*, **32** (9) 1237-1242.

Sundström, B. 1998. “*Handbok och formelsamling i hållfasthetslära*”, Institutionen för hållfasthetslära KTH, Stockholm, Sweden.

Tan, S.C. 1994. ”*Stress concentrations in laminated composites*”, Technomic, Basel, Switzerland.

Xiong, Y. 1994. “On the finite width correction factor in composite laminates with elliptical inclusion”, *Advanced Composites Letters*, **3** (6) 203-207.

Xiong, Y., Poon, C., Straznicky, P.V. and Vietinghoff, H. 1995. “A prediction method for the compressive strength of impact damaged composite laminates”, *Composite Structures*, **30** (4) 357-367.

Zenkert, D. and Battely, M. 1996. “*Foundations of fibre composites*”, Paper 96-10, Royal Institute of Technology, Department of Aeronautics, Stockholm, Sweden.

Acknowledgements

I would like to thank the people at the Aeronautical Research Institute of Sweden, FOI/FFA who have helped me with this thesis. The comments and advice from my thesis advisor, Dr. Robin Olsson, have been appreciated and often essential for my work. Dr. Gunnar Melin is also acknowledged for his tremendous help with the optical equipment.

Thorvald Linderoth, Bengt Wallstenius and Kjell Welin are also gratefully acknowledged for their assistance in the laboratory.

Appendix A. Failure data, tension

Table A.1 Maximum stress and strain, tension.

Specimen	Max. stress [MPa] σ_N^∞		Far-field strain [%]	
	Gage [1]	DSP [2]	Gage [3]	DSP [4]
T000/5-1	409		0.68	
T000/5-2	398		0.69	
T000/5-3	407		0.70	
T000/10-1	377	373	0.65	0.69
T000/10-2	372	369	0.63	0.67
T000/10-3	377	373	0.66	0.74
T000/20-1	319	319	0.55	0.62
T000/20-2	323	323	0.57 [5]	0.58
T000/20-3	326	325	0.56	0.57
T020/20-1	339	178 [6]		0.33 [6]
T020/20-2	343	156 [6]		0.31 [6]
T020/20-3	333	197 [6]		0.34 [6]
TCUT/10-1	438	433	0.80	0.81
TCUT/10-2	422	422	0.73	[7]
TCUT/10-3	418	418	0.77	[7]
TCUT/20-1	402	403	0.73 [5]	0.78
TCUT/20-2	413	412	0.74	0.80
TCUT/20-3	398	396	0.72	0.68
T100/0-1	832		1.50	
T100/0-2	811		1.49	
T100/0-3	841		1.57	

[1]: Maximum stress measured with the test machine.

[2]: Stress at the last step measured with the DSP.

[3]: Average maximum strain of gage 3 and 4 (see Figure 4.1).

[4]: ε_{ff}, curve fit approximation as $x \to \infty$ of the calculated average strain at the last step of the DSP.

[5]: One gage damaged.

[6]: Last step before release of the inclusion.

[7]: Large damage zone, no reliable results.

Appendix B. Failure data, compression

Table B.1 Maximum stress and strain, compression.

Specimen	Max. stress [MPa] σ_N^∞		Far-field strain [%]	
	Gage [1]	DSP [2]	Gage [3]	DSP [4]
C000/5-1	337		0.60	
C000/5-2	344		0.62	
C000/5-3	360		0.60	
C000/10-1	310	307	0.54	0.66
C000/10-2	334	332	0.60	0.73
C000/20-1	286	280	0.51	0.54
C000/20-2	268	268	0.47	0.44
C020/5-1	483		0.78	
C020/5-2	443		0.77	
C020/5-3	496		0.82	
C020/10-1	399	398	0.76	0.79
C020/10-2	398	395	[5]	0.79
C020/20-1	346	344	0.63	0.68
C020/20-2	340	337	0.65 [6]	0.59
CCUT/10-1	429	428	0.85	0.92
CCUT/10-2	420	420	0.85	0.92
CCUT/20-1	408	405	0.86	0.84
CCUT/20-2	384	379	0.78 [6]	0.78
C100/0-1	615		1.29	
C100/0-2	584		1.20	
C100/0-3	552		1.11	

[1]: Maximum stress measured with the test machine.

[2]: Stress at the last step measured with the DSP.

[3]: Average maximum strain of gage 3 and 4 (see Figure 4.1).

[4]: ε_{ff}, curve fit approximation as $x \to \infty$ of the calculated average strain at the last step of the DSP.

[5]: Both gages damaged.

[6]: One gage damaged.

Appendix C. Strain distribution in the laminate

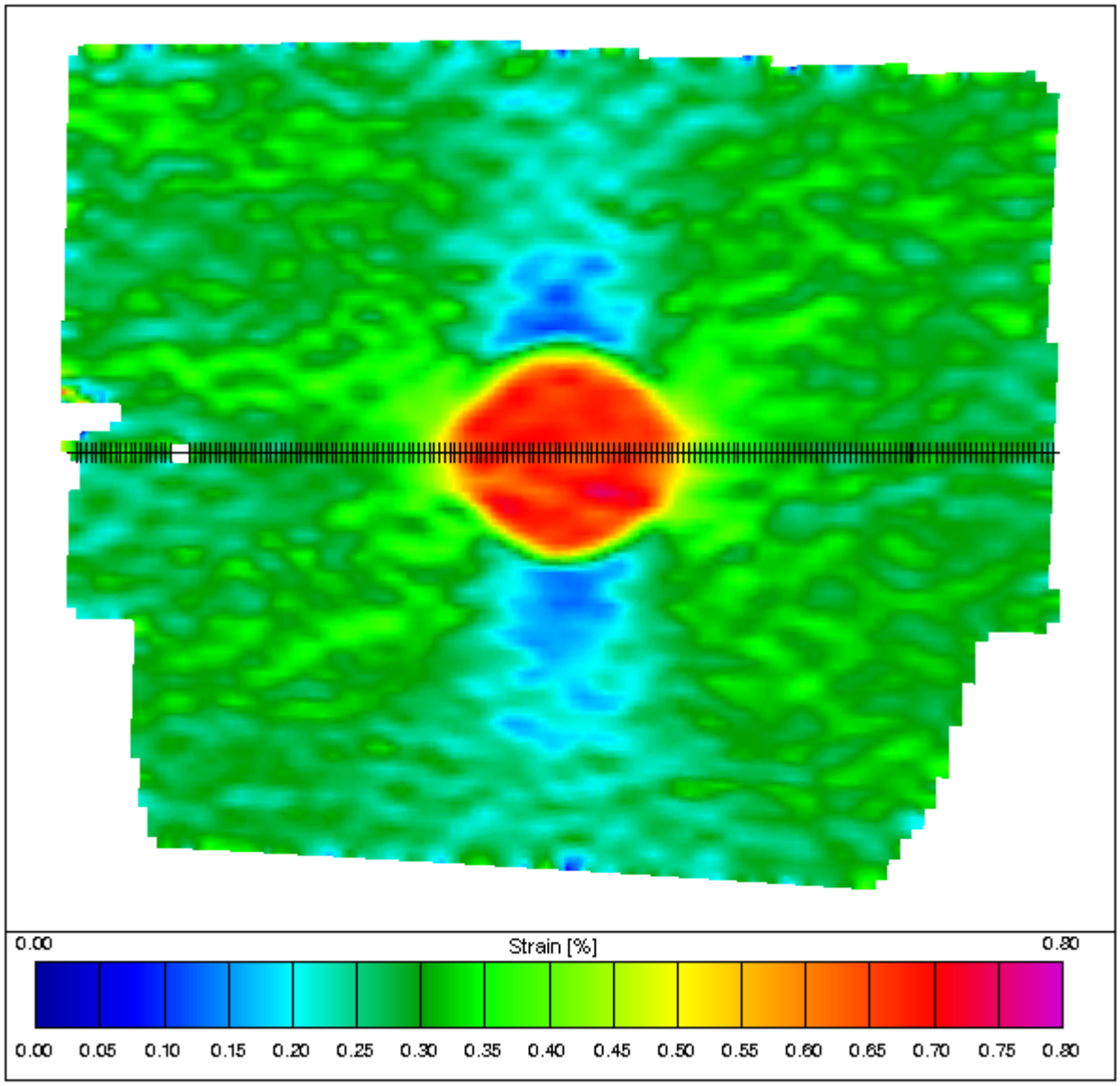

Figure C.1 Example of results for a tension test with a 20 mm inclusion presented as a color map of the strain in the loading direction. The strain distribution along the black line is shown in Figure 5.4. (Specimen T020/20-2, with 23 mm lens. σ^{∞} = 156 MPa.)

Appendix D. Strain distribution in the inclusion

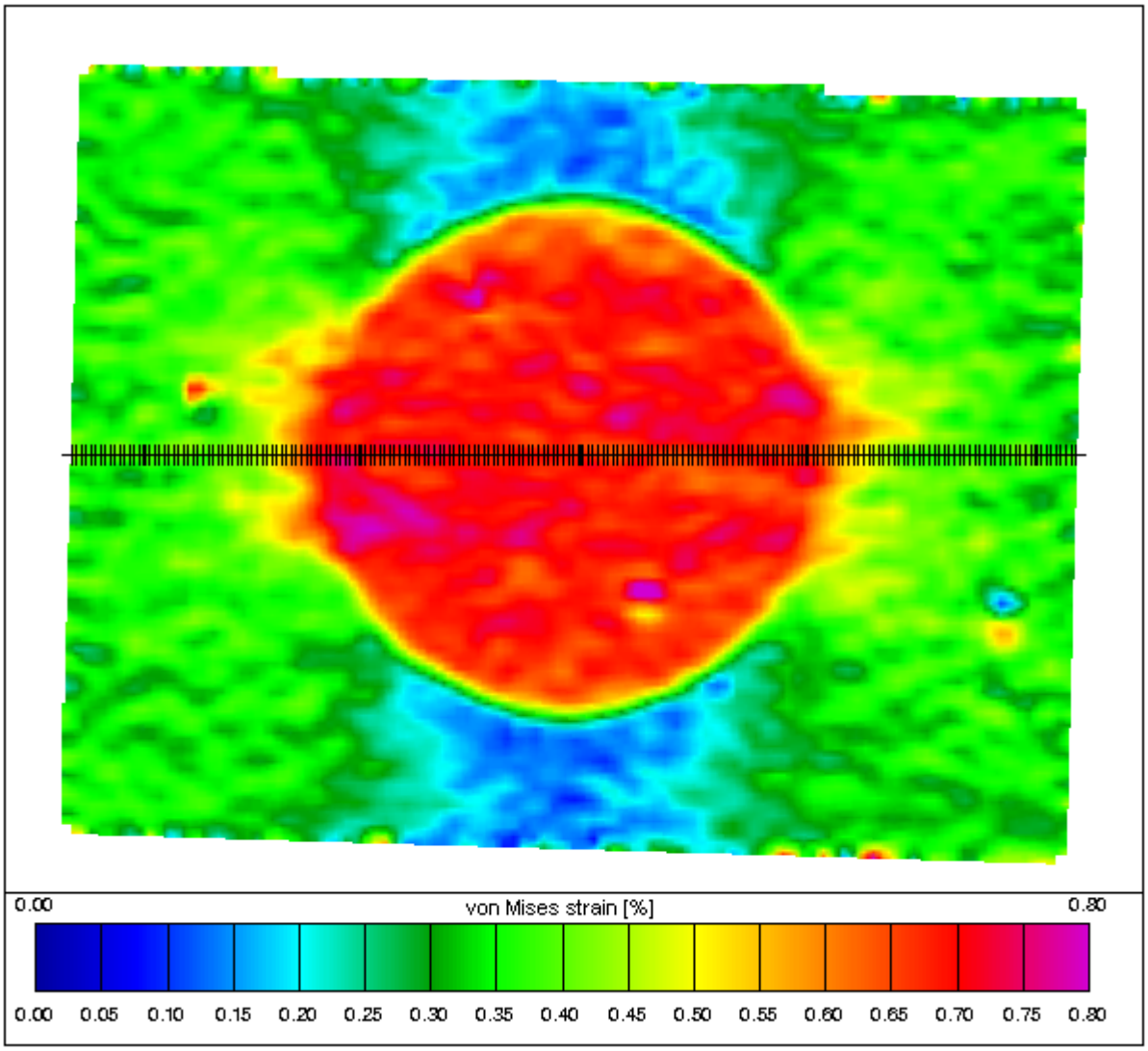

Figure D.1 von Mises strain for a tension test with a 20 mm inclusion, results from the opposite side of the specimen in Figure C.1. Note the homogenous strain in the inclusion. (Specimen T020/20-2, with 50 mm lens. σ^{∞} = 156 MPa.)